Journal of
METAMORPHIC GEOLOGY

J. metamorphic Geol., 2014, **32,** 71–92 doi:10.1111/jmg.12059

Intragrain oxygen isotope zoning in titanite by SIMS: Cooling rates and fluid infiltration along the Carthage-Colton Mylonite Zone, Adirondack Mountains, NY, USA

C. E. BONAMICI, R. KOZDON, T. USHIKUBO AND J. W. VALLEY
Department of Geoscience, WiscSIMS, University of Wisconsin-Madison, 1215 Dayton St., Madison, WI, 53706, USA (chloebee@lanl.gov)

ABSTRACT Oxygen isotopes are an attractive target for zoning studies because of the ubiquity of oxygen-bearing minerals and the dependence of mineral $^{18}O/^{16}O$ ratios on temperature and fluid composition. In this study, subtle intragrain oxygen isotope zoning in titanite is resolved at the 10-μm scale by secondary ion mass spectrometry. The patterns of $\delta^{18}O$ zoning differ depending on microstructural context of individual grains and reflect multiple processes, including diffusive oxygen exchange, partial recrystallization, grain-size reduction, and grain growth. Using the chronological framework provided by structural relations, these processes can be related to specific events during the Grenville orogeny. Titanite was sampled from two outcrops within the Carthage-Colton Mylonite Zone (CCMZ), a long-lived shear zone that ultimately accommodated exhumation of the Adirondack Highlands from beneath the Adirondack Lowlands during the Ottawan phase (1090–1020 Ma) of the Grenville orogeny. Titanite is hosted in the Diana metasyenite complex, which preserves three sequentially developed fabrics: an early NW-dipping protomylonitic fabric (S_1) is crosscut by near-vertical ultramylonitic shear zones (S_2), which are locally reoriented by a NNW-dipping mylonitic fabric (S_3). Texturally early titanite (pre-S_2) shows diffusion-dominated $\delta^{18}O$ zoning that records cooling from peak Ottawan, granulite-facies conditions. Numerical diffusion models in the program Fast Grain Boundary yield good fits to observed $\delta^{18}O$ profiles for cooling rates of 50 ± 20 °C Ma^{-1}, which are considerably faster than the 1–5 °C Ma^{-1} cooling rates previously inferred for the Adirondack Highlands from regional thermochronology. High cooling rates are consistent with an episode of rapid shearing and exhumation along the CCMZ during gravitational collapse of the Ottawan orogen at *c.* 1050 Ma. Texturally later titanite (syn-S_2) has higher overall $\delta^{18}O$ and shows a transition from diffusion-dominated to recrystallization-dominated $\delta^{18}O$ zoning, indicating infiltration of elevated-$\delta^{18}O$ fluids along S_2 shear zones and continued shearing below the blocking temperature for oxygen ($\sim\leq$500 °C for grain sizes at the study site). The texturally latest titanite (post-S_3) has growth-dominated $\delta^{18}O$ zoning, consistent with porphyroblastic grain growth following cessation of shearing along the Harrisville segment of the CCMZ.

Key words: Adirondack Mountains; Grenville; oxygen isotopes; titanite; zoning.

INTRODUCTION

Grain-scale zoning presents an inherent opportunity to understand details of changing *P–T–X*(fluid) conditions, provided that zoned compositional constituents can be measured with sufficient precision and accuracy at the desired (usually sub-mm) spatial resolution. Precise, high-spatial-resolution, in situ characterization of major- and minor-element zoning is routine, but high-spatial-resolution, in situ characterization of isotopic zoning is less common. Continuing advances in secondary ion mass spectrometry (SIMS) techniques allow for increasingly accurate and precise intragrain analyses of isotopes, for example (Kita *et al.*, 2009; Harrison *et al.*, 2010; Hartley *et al.*, 2012; Schmitt & Zack, 2012).

Oxygen isotopes are an attractive geochemical target for zoning studies because (i) oxygen is the major element in most Earth minerals; (ii) isotope exchange does not change the total concentration of oxygen within a mineral; and (iii) oxygen isotope ratios can vary strongly as a function of temperature and fluid composition. Oxygen isotope ratios have been used to investigate thermal histories and fluid regimes in metamorphic rocks for more than 50 years (Urey, 1947; Valley, 2001). Minerals incorporate isotopes of oxygen in different proportions as a function of crystal structure, composition, system (bulk rock) composition and temperature (e.g., Chacko *et al.*, 2001). Isotopic potential gradients arise within and between phases because the masses of bonded atoms affect the vibrational contribution

to the total free energy of a phase. Oxygen isotope exchange equilibria can therefore be written in a manner exactly analogous to chemical exchange equilibria. Theoretically, the advantage of oxygen isotope exchange equilibria is that any two oxygen-bearing minerals may be utilized as a thermometry pair, provided the minerals attained and preserved isotopic equilibrium (Valley, 2001).

Although isotopic potential gradients are thermodynamic phenomena, mass transfer (whether of chemical or isotopic species) is fundamentally a kinetic process. Consequently, oxygen isotope equilibrium is not always attained at peak temperature or maintained during cooling, and oxygen isotope zoning, like chemical zoning, may develop at a variety of spatial scales. Workers have characterized oxygen isotope zonation at the map-scale (Lackey & Valley, 2004; Peck *et al.*, 2004), outcrop scale (Cartwright *et al.*, 1993; Gerdes *et al.*, 1995; Abart & Pozzorini, 2000; Nabelek, 2002), thin-section scale (Eiler *et al.*, 1995a; Bowman *et al.*, 2009; Ferry *et al.*, 2011), and, increasingly, at the grain scale (Eiler *et al.*, 1993; Kohn *et al.*, 1993; Eiler *et al.*, 1995b; Cole *et al.*, 2004; Ferry *et al.*, 2010; Bonamici *et al.*, 2011; D'Errico *et al.*, 2012; Raimondo *et al.*, 2012).

In this contribution, we demonstrate that subtle intragrain $\delta^{18}O$ variations in titanite can be resolved by SIMS at the 10-μm scale and that the type of $\delta^{18}O$ zoning is correlated to the structural setting of the titanite grain. Combining micron-scale *in situ* geochemical characterization with microstructural and mesostructural observations, we show that $\delta^{18}O$ zoning in titanite records high-temperature geological events, including shear-zone development, fluid infiltration, and Grenville-aged tectonic exhumation.

STUDY LOCALE AND PREVIOUS WORK

The Adirondack Mountains expose multiply deformed meta-igneous and metasedimentary rocks of the Grenville tectonic cycle (*c.* 1350–900 Ma). The NW Adirondack Lowlands and central Adirondack Highlands are juxtaposed across the Carthage-Colton mylonite zone (CCMZ), a major, NE-striking structure (Fig. 1a,b). The relative position of the Highlands and Lowlands during the early Ottawan phase of the Grenville orogeny and the timing of their current structural juxtaposition remain controversial (Wiener, 1983; Streepey *et al.*, 2000; Baird & MacDonald, 2004); however, the CCMZ ultimately accommodated NW-directed normal-sense displacement of the Adirondack Lowlands and exhumation of the Adirondack Highlands during the 1090–1020 Ma Ottawan phase of the Grenville Orogeny (Mezger *et al.*, 1992; Streepey *et al.*, 2001; Selleck *et al.*, 2005). Deformation along the CCMZ initiated in the middle crust at amphibolite–granulite facies conditions (Mezger *et al.*, 1991a; Cartwright *et al.*, 1993; Streepey *et al.*, 2001; Baird & MacDonald, 2004; Chappell *et al.*, 2006). Peak metamorphism in the NW Lowlands occurred at *c.* 1150 Ma, whereas the Highlands record peak metamorphic conditions at *c.* 1050 Ma (Mezger *et al.*, 1991a, 1992; McLelland & Daly, 1996; McLelland *et al.*, 2001). U-Pb dating of metamorphic vein titanite (by TIMS and SHRIMP-RG) from the Diana metasyenite near Harrisville, New York, yields ages from 1089 to 1022 Ma, with a *c.* 1050 Ma age population peak that likely dates the onset of predominantly normal-sense shearing along the CCMZ (Heumann, 2004; Chappell *et al.*, 2006).

Our work builds upon the previous findings of Cartwright *et al.* (1993), who measured $\delta^{18}O$ on whole-rock and mineral-separate samples from two large outcrops of Diana metasyenite near Harrisville (Fig. 1c), the same outcrops on which this study is based. U-Pb zircon ages indicate that the protolith syenite was intruded at 1164 ± 12 Ma as a part of the regional anorthosite-mangerite-charnockite-granite (AMCG) plutonic suite (Hamilton *et al.*, 2004). Subsequently, Ottawan metamorphism with peak conditions of 650–700 °C and 6–7 kbar (Bohlen *et al.*, 1985; Cartwright *et al.*, 1993; Gerdes & Valley, 1994; Kitchen & Valley, 1995) stabilized the assemblage alkali feldspar (perthite) + plagioclase + quartz + augite + titanite + magnetite ± ilmenite ± hornblende in the metasyentite. Cartwright *et al.* (1993) documented systematic differences in whole rock and mineral $\delta^{18}O$ values between the metasyenite and cm-scale shear zones that crosscut the metasyenite. They reported both shear zones with low $\delta^{18}O$ values, which they attributed to interactions with meteoric fluids, and shear zones with elevated $\delta^{18}O$ values, which they attributed to interactions with high-$\delta^{18}O$ fluids coming from nearby marbles. Magnetite-ilmenite oxybarometry and mineral-pair oxygen isotope thermometry also revealed a correlation between the degree of late isotope exchange and degree of shearing (Cartwright *et al.*, 1993). Some of the cm-scale shear zones are developed within or along the margins of steeply dipping, crosscutting veins with abundant augite + alkali feldspar ± quartz ± scapolite ± titanite ± calcite. Petrographic investigation reveals that titanite is a widespread accessory phase, present within shear zones, adjacent wallrock, and augite-rich veins.

MESOSTRUCTURE

The two main Harrisville area roadcuts are large (~400 and 800 m in length × 3–20 m high), fresh, ENE- to NE-striking subvertical exposures through the Diana metasyenite. The roadcuts are approximately three kilometres apart and both are located within 200 m of the contact of the Diana metasyenite with regionally extensive marbles of the Adirondack Lowlands (Fig. 1b,c). For ease, the larger easternmost roadcut is referred to as the eastern

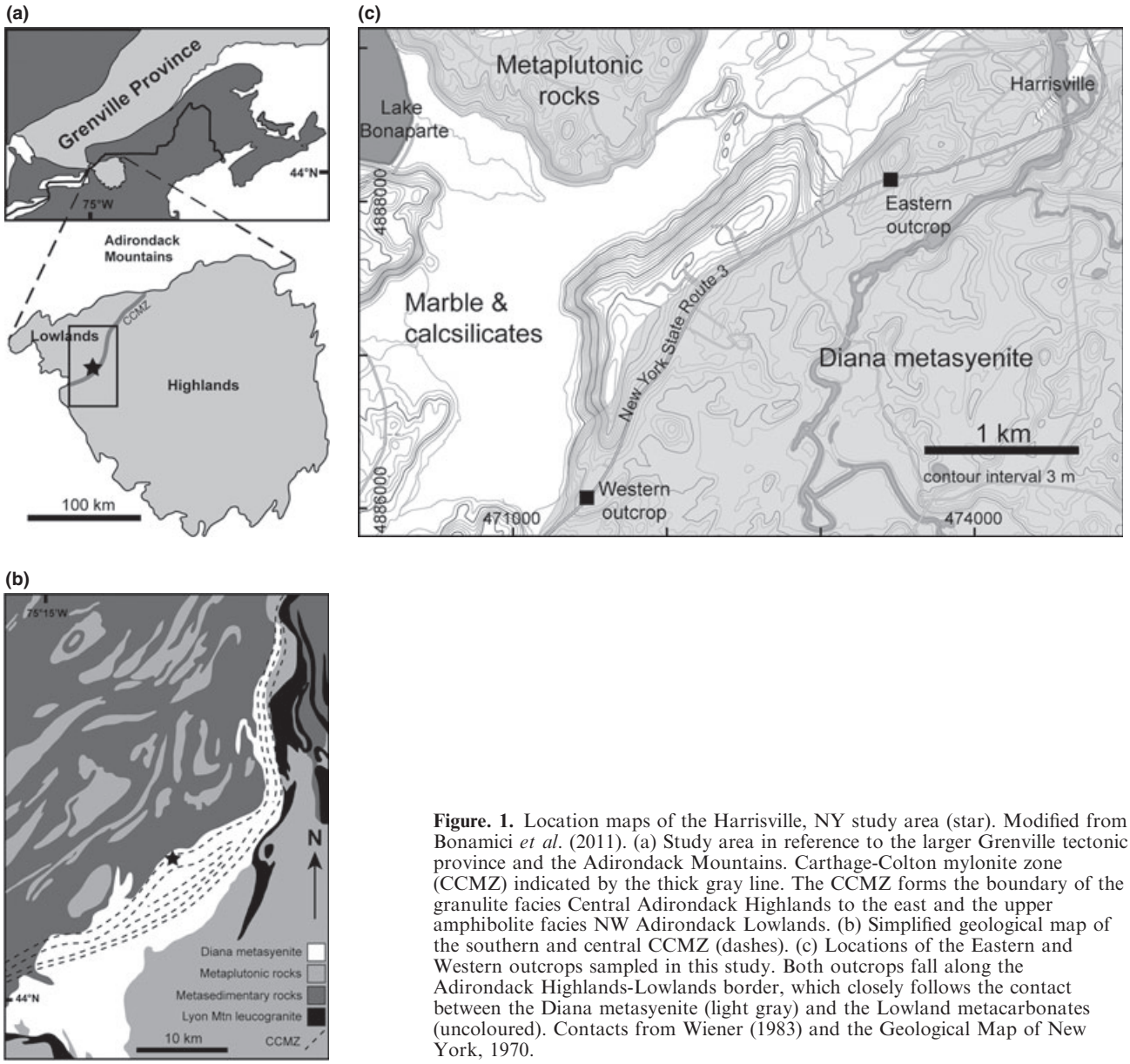

Figure. 1. Location maps of the Harrisville, NY study area (star). Modified from Bonamici *et al*. (2011). (a) Study area in reference to the larger Grenville tectonic province and the Adirondack Mountains. Carthage-Colton mylonite zone (CCMZ) indicated by the thick gray line. The CCMZ forms the boundary of the granulite facies Central Adirondack Highlands to the east and the upper amphibolite facies NW Adirondack Lowlands. (b) Simplified geological map of the southern and central CCMZ (dashes). (c) Locations of the Eastern and Western outcrops sampled in this study. Both outcrops fall along the Adirondack Highlands-Lowlands border, which closely follows the contact between the Diana metasyenite (light gray) and the Lowland metacarbonates (uncoloured). Contacts from Wiener (1983) and the Geological Map of New York, 1970.

outcrop, whereas the smaller roadcut to the west is called the western outcrop. These outcrops were referred to as the Pyramid and the Wave, respectively, by Cartwright *et al*. (1993). Rock exposures cannot be traced continuously from the Eastern outcrop to the Western outcrop, but a set of distinctive millimetre- to centimetre-scale ultramylonite shear zones occur in both outcrops (Fig. 2a), allowing structural correlation between them despite their separation. Three fabrics are recognized between the two outcrops and their relative ages are determined from observed and inferred crosscutting relations (Fig. 2f).

The oldest fabric (S_1) is represented by the pervasive weakly to moderately developed, moderately NW-dipping protomylonite that dominates the eastern road cut (Fig. 2b,e). This fabric is defined by grain-shape preferred orientation of partially recrystallized feldspar porphyroclasts and wispy lenses of mafic phases, including augite, hornblende, ilmenite, magnetite and titanite. S_1 foliation surfaces undulate at the centimetre and metre scale and no stretching lineation was identified.

The S_1 protomylonite of the eastern outcrop is crosscut by at least 136 millimetre- to centimetre-scale, steeply dipping ultramylonitic shear zones (S_2; Fig. 2a–c). The fabric within S_2 shear zones is a compositional banding defined by lenses of recrystallized felsic and mafic minerals and is parallel to the typically sharp shear zone boundaries. S_2 shear zones

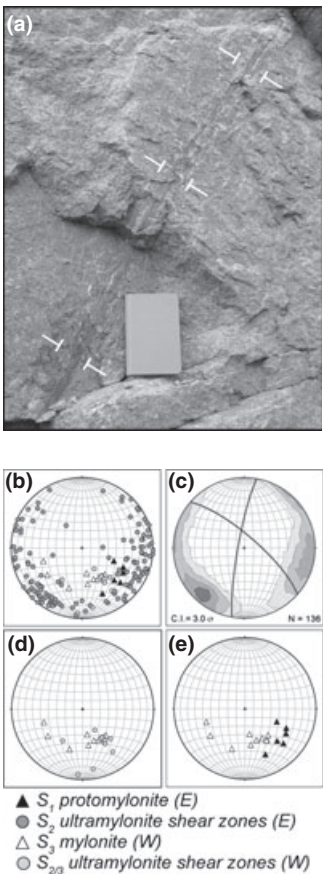

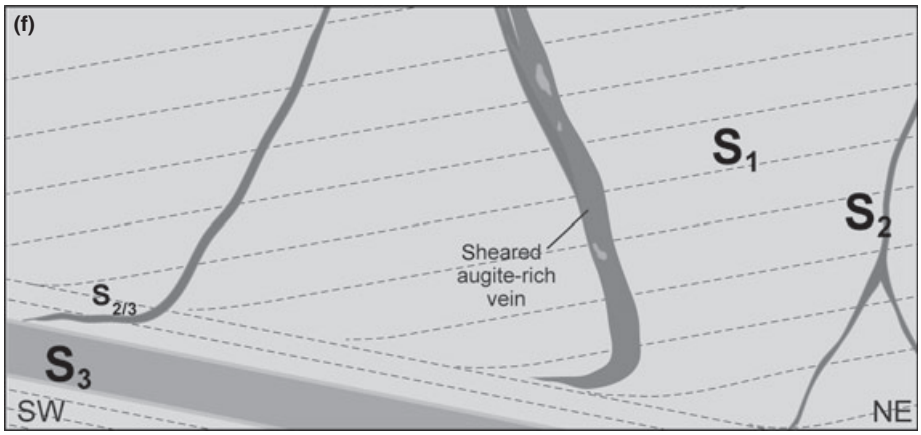

Fig. 2. Structure in the Diana metasyenite at the Harrisville site. All data are shown as poles to foliation plotted on lower-hemisphere equal area nets. (a) Field photograph of an S_2 ultramylonitic shear zone (brackets) crosscutting the protomylonitic metasyenite wallrock of the eastern outcrop. (b) All fabric measurements from the Harrisville outcrops. (c) Contoured poles to foliation of S_2 shear zones and representative planes (black great circles) showing the two dominant shear zone orientations. (d) Orientations of the S_3 mylonitic wallrock fabric and ultramylonitic shear zones in the western outcrop. (e) Comparison of wallrock fabric orientations at the eastern (blue triangles) and the western (orange triangles). (f) Cartoon summary vertical cross-section (looking to the northwest) of the interpreted structural relations in the two Harrisville outcrops. S_1 and S_2 fabrics are observed in the eastern outcrop, whereas the S_3 fabric, including inferred transposed $S_{2/3}$ shear zones, are observed in the western outcrop. Dark gray represents variably sheared augite-rich veins containing cm-scale titanite (lighter gray lenses).

widen and merge in Y-shaped junctions or, rarely, in X-shaped junctions with no observable offset of either shear zone. These relations indicate that the shear zones formed contemporaneously as an anastomosing network. Although shear zone strike is variable, orientations cluster into NNE- and NW-striking groups that broadly define a 60/120° geometry (Fig. 2c). Several S_2 shear zones are developed along the margins of or within steeply dipping, cm- to m-wide augite-rich veins (Heumann, 2004; Chappell *et al.*, 2006) that also crosscut the S_1 fabric at a high angle (Fig. 2f). The orientation of the veins and their spatial association with the S_2 shear zones indicates contemporaneous vein emplacement and shearing, and we consider veins to be part of the S_2 fabric. In fact, most veins are deformed by S_2 shear zones, and some veins are attenuated to the extent that only small pods, lenses and discontinuous layers of vein material, recognized by aggregates of deep green subcalcic augite ± pink alkali feldspar, survive within the shear zone.

In the western outcrop, cm-thick ultramylonitic shear zones either crosscut at a low angle or parallel a well-developed penetrative mylonitic fabric (Fig. 2b,d,e). We infer that these are transposed S_2 shear zones, and that the wallrock mylonite is therefore a later generation of fabric (S_3). The S_3 fabric is defined by grain-shape preferred orientation of feldspar porphyroclasts, quartz ribbons, and thin lenses of grain-size reduced mafic phases. Locally, S_3

Fig. 3. Images of representative microstructures for the four Types of titanite. All scale bars are 1 mm unless otherwise indicated. All images are transmitted light photomicrographs except (b). (a) T1. Lens of fine-grained augite + quartz + titanite + magnetite between porphyroclasts of alkali feldspar in S_1 protomylonite. (b) T1. BSE image of a rare ~500 μm-long titanite grain within a lens as shown in (a). Backscatter contrast is focused over a narrow range to show subtle zoning in titanite. Typical bright rim indicated with white arrow. (c) T2. Ovoid titanite porphyroclasts within an ultramylonitic S_2 shear zone. (d) T2. Foliation in the grain-size reduced matrix wrapping a large titanite porphyroclast with dusty-appearing ilmenite inclusions. Quarter fold at upper right indicates dextral shear in the plane of the thin section. (e) T3. Titanite porphyroclast within a sheared augite-rich vein. (f) T3. Cross-polarized image of cm-scale vein titanite showing segmentation of the grain into cores surrounded by fine-grained recrystallized rims. Cores commonly contain deformation twins, which appear as irregular, lighter gray bands in this image. Nearly entire field of view is titanite. (g) T4. Xenoblastic titanite and augite porphyroblasts overgrowing S_3 (ultra)mylonite. (h) T4. Cross-polarized image of titanite porphyroblast. Compare the average S_2 matrix grain size in (d) with the average S_3 matrix grains size.

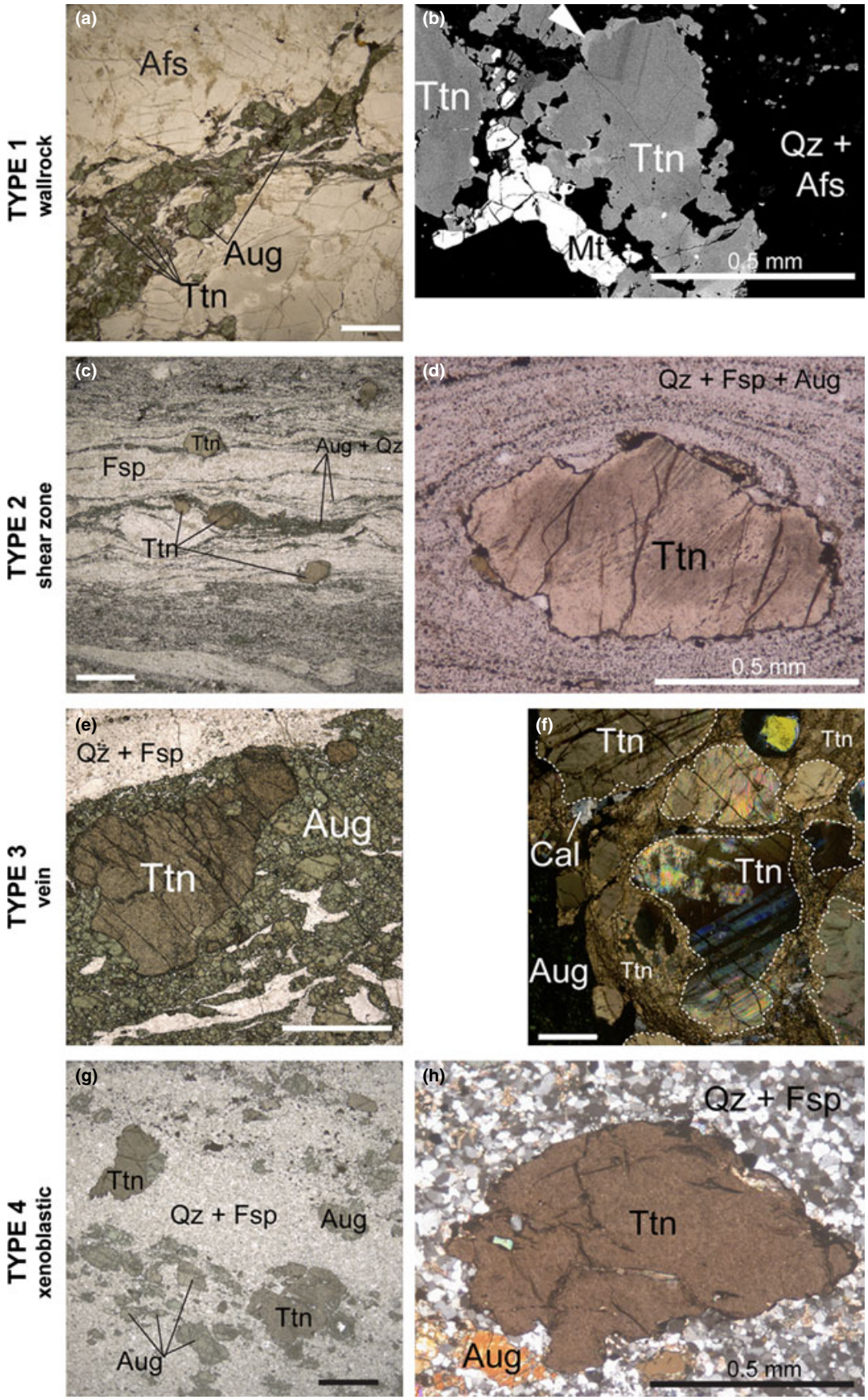

mylonite grades into metre-thick layers of ultramylonite. These ultramylonite zones differ from the S_2 ultramylonitic shear zones in that they are wider, exhibit gradational rather than sharp boundaries, are coarser grained, and contain abundant xenoblastic titanite (Type-4 titanite, described below). The widest S_3 ultramylonite zone contains a higher modal abundance of quartz than the adjacent metasyenite mylonite, suggesting that it was localized in a slightly different lithological facies of the Diana metasyenite complex. Both S_3 mylonitic fabric and transposed S_2 shear zones of the Western outcrop dip more gently than and are rotated systematically 10–60° clockwise relative to the eastern outcrop S_1 protomylonite (Fig. 2e).

MICROSTRUCTURE

Within the two Harrisville outcrops, there are four distinct occurrences of titanite on the basis of microstructural context (Fig. 3; Table 1). These types are (i) wallrock titanite grains; (ii) shear zone titanite porphyroclasts (iii) vein-related (variably sheared) titanite grains; and (iv) titanite xenoblasts. Types-1, -2 and -3 occur exclusively at the Eastern outcrop, whereas Type-4 titanite occurs exclusively at the Western outcrop. A relative chronology of development has been determined from a combination of microstructural characteristics and relations to the mesoscale structures and fabrics described above. The different occurrences or types of titanite are described below in order of relative age from oldest to youngest.

Type 1: Wallrock titanite (Eastern outcrop)

Type-1 (T1) titanite occurs as ≤500-μm anhedral grains with curviplanar or lobate boundaries occurring within thin lenses of mafic minerals that define the S_1 protomylonitic fabric of the eastern outcrop (Fig. 3a). The lenses comprise aggregates of augite + titanite + magnetite + zircon ± hornblende ± ilmenite. Most T1 titanite grains larger than 200 μm exhibit undulatory to patchy extinction. Some grains are mantled by thin rims of fine-grained titanite and many occur as trains of ≤100 μm grains, suggesting that most T1 grains predate S_1 and underwent some degree of grain-size reduction during development of S_1 protomylonite. Augite shows similar microstructural features indicating that it also underwent grain-size reduction. In backscattered electron (BSE) images, titanite exhibits faint oscillatory to patchy zoning that is commonly truncated by higher Z rims (Fig. 3b).

Type 2: Shear-zone titanite (Eastern outcrop)

The Type-2 (T2) titanite category includes all grains sampled from S_2 ultramylonitic shear zones *not* associated with augite-rich veins. At the microscale, S_2 shear-zone foliation is a compositional layering defined by elongate strings and lenses of grain-size reduced mafic and felsic phases. T2 titanite occurs as ~200–1500 μm ovoid porphyroclasts 'wrapped' by S_2 foliation (Fig. 3c,d). T2 grains commonly show preferred orientation with the longer grain dimension parallel or subparallel to shear zone foliation (Fig. 3d). In a few samples, titanite grains are asymmetric winged porphyroclasts, and smaller anhedral titanite grains can be traced back along specific foliation trajectories to nearby larger grains where they appear to have originated. Many, if not most, grains larger than ~500 μm exhibit undulatory extinction and/or tapering lamellar twins. In BSE images, T2 grains display very faint patchy zoning and one or more rims of variable thickness and continuity.

Type 3: Vein-associated titanite (Eastern outcrop)

Type-3 (T3) titanite grains include variably recrystallized centimetre-scale porphyroblasts (up to 5 cm-long) within augite-rich veins (Fig. 3e,f) and smaller, 500–2000 μm grains associated with augite + mesoperthite aggregates strung out along S_2 shear zones. Many of the smaller grains represent survivors of vein attenuation within shear zones. Similar orientations and strong spatial association of augite-rich veins within S_2 shear zones suggests that veins, and therefore T3 titanite grains, formed contemporaneously with S_2 shear zones. Most cm-scale titanite forms aggregates of smaller grains which have well-developed core-and-mantle structure (Fig. 3f). Many of the grain cores exhibit undulose extinction, fractures, and/or tapered lamellar twins. Grains with a cloudy or speckled appearance contain μm-scale inclusions and voids, consistent with crystallization in the presence of fluids. In high-contrast BSE images, T3 grains typically display sharp, patchy and/or irregular concentric zoning. Irregular concentric zoning with lobate, embayed or distinctly non-planar zone boundaries is well-developed in most centimetre-scale titanite grains.

Type 4: Xenoblastic titanite (Western outcrop)

The Western outcrop wallrock mylonite lacks titanite but grades into metre-thick zones of ultramylonite that contain abundant xenoblastic mm-scale titanite grains (Fig. 3g). These Type-4 (T4) titanite grains are ~500–2000 μm long with irregular rims that overgrow the late, moderately dipping S_3 ultramylonite zone foliation (Fig. 3g,h). In BSE images, titanite grains typically display patchy zoning with both gradational and sharp zone boundaries (Fig.8b). The grain-size reduced quartz-and-feldspar-dominated matrix shows textural evidence for recovery following dynamic recrystallization, including smoothly curviplanar

Table 1. Summary of study samples from the Diana metasyenite in the vicinity of Harrisville, New York.

Outcrop	UTM coordinates[1] E	UTM coordinates[1] N	SIMS mount	Grain number	Grain type	Fabric relations	Rock type
E	473365	4888118	09HA12B	T1.1	1	pre-S_2	Protomylonite
E	473526	4888153	09HA03AB	T1.2	1	pre-S_2	Protomylonite
E	473391	4888132	09HA09A2	T2.1	2	pre-S_2	Ultramylonite
E	473526	4888153	09HA03A	T2.2	2	pre-S_2	Ultramylonite
E	473526	4888153	09HA03A	T2.3	2	pre-S_2	Ultramylonite
E	473391	4888132	09HA09A	T2.4	2	pre-S_2	Ultramylonite
E	473365	4888118	09HA12A	T3.1	3	syn-S_2	Sheared augite vein
E	473389	4888125	09HA18	T3.2	3	syn-S_2	Augite + apatite vein
E	473509	4888155	09HA08A	T3.3	3	late-syn-S_2	Sheared augite vein
E	473509	4888155	09HA07B	T3.4	3	syn-S_2	Sheared augite vein
E	473509	4888155	09HA07B	T3.5	3	syn-S_2	Sheared augite vein
W	471389	4885954	09HA13A	T4.1	4	pre-S_2 core, post-S_3 rims	Ultramylonite
W	471389	4885954	09HA13A	T4.2	4	pre-S_2 core, post-S_3 rims	Ultramylonite

[1]NAD83/UTM zone 18T.

grain boundaries (Fig. 3h). Compositional layering on the scale of the thin-section is defined by differences in the relative abundance of quartz and augite. In general, there is a significantly higher abundance of quartz in samples with T4 titanite grains.

MICROANALYTICAL METHODS

Sample mounts were prepared from petrographic thin sections of the Harrisville samples in order to preserve the microstructural context of each titanite grain and ensure that grain rims were intact. Sections were polished to achieve <1 μm of surface relief, cut into 25-mm diameter rounds, and carbon coated.

The intragrain chemical zoning in the Harrisville titanite was characterized by wavelength dispersive spectroscopy, using the University of Wisconsin Cameca SX-51 electron microprobe. Point analyses were collected adjacent (within 10–30 μm) to every SIMS $\delta^{18}O$ pit along cross-grain traverses in order to correct for SIMS analytical bias (see below), and these analyses generate a complementary EPMA traverse for each SIMS traverse. Point analyses were performed with a 15 keV accelerating voltage, 40 nA beam, and $\leq$1 μm beam diameter. Counts were collected for 14 major (Ca, Ti, Si), minor (Al, Fe, Na, Mg, Mn, F), and trace elements (Zr, Hf, Y, Ce, Nd) with 10 s peak and 5 s background counting times. A significant Si Kα peak shift was observed in titanite relative to the jadeite standard and thus the Si peak position for all analyses is based on the Renfrew titanite standard. ZAF corrections and data reduction were performed with Probe for EPMA software (Donovan *et al.*, 2009). ZAF corrections are based on measured fluorine and stoichiometric oxygen assuming no OH^- substitution, though some amount of OH must be present in all Harrisville titanite. To avoid the issue of exact anion site occupancy, cation formula atoms were calculated by assuming that all cations sum to fill three sites per formula unit. Fe is assumed to be Fe^{3+}. All EPMA data are tabulated in Table S1.

All $\delta^{18}O$ measurements were made on the WiscSIMS Cameca IMS-1280 ion microprobe with a 1.8–2.2 nA Cs^+ primary beam (Table S2). The instrument was tuned using standard operating conditions and procedures for oxygen two-isotope analyses detailed in (Kita *et al.*, 2009). Analysis pits were slightly ovoid and 10–17 μm in diameter (longest dimension) by 1 μm deep. Oxygen isotope profiles were generated for each titanite grain through a series of closely spaced analyses along cross-grain or, in the case of very large cm-scale grains, rim-to-core traverses.

Data were acquired over the course of 10 different analytical sessions; instrumental bias was calibrated for each session by analyzing a suite of titanite standards and drift was monitored throughout the session by repeated analyses of a quartz standard embedded in each sample mount. Previous work (Bonamici *et al.*, 2011) established that instrumental bias occurring during the ion microprobe measurement of $\delta^{18}O$ in titanite correlates linearly with the abundance of Ti in the octahedral site over the compositional range of interest (~0.75–1.0 formula atoms Ti). A suite of three chemically (major and minor elements) and isotopically ($\delta^{18}O$) homogeneous natural titanite standards (Renfrew titanite, Khan Mine titanite, and Tiburon 3 titanite; Tables S3 & S4) were measured and bracketed by analyses of the quartz standard (UWQ-1, $\delta^{18}O$ = 12.33 ‰VSMOW; Kelly *et al.*, 2007) during each analytical session. Each set of 10-15 titanite $\delta^{18}O$ sample analyses was also bracketed by 8–12 analyses of UWQ-1. The spot-to-spot precision for the unknown measurements is calculated as twice the standard deviation of the 8-12 UWQ-1 measurements that bracket each set of sample analyses. Following SIMS analysis, quantitative EPMA compositional data were collected within 10–30 μm of every SIMS pit in order to calculate Ti for-

mula atoms (Table S1) for the instrumental bias correction. Formula-atom calculations were made by normalizing to three cations to minimize the effect of uncertainties in the anion composition on the bias calculation. All SIMS $\delta^{18}O$ data are tabulated in Table S2 and bias correction curves for each analytical session are compiled in Fig. S1.

TITANITE CHEMICAL COMPOSITION AND ZONING

The variety of titanite microstructures and their relations to structures described above suggests more than one petrogenetic origin for the Harrisville titanite grains. The T1 wallrock microstructures discussed above indicate that at least some, and possibly many, of the Harrisville titanite grains originated as magmatic crystals in the 1164 ± 12 Ma Diana syenite (Hamilton *et al.*, 2004). Magmatic titanite is common in slowly cooled, oxidized plutons (Xirouchakis *et al.*, 2001a), which is consistent with the high titanite $\delta^{18}O$ (see below) and whole-rock $\delta^{18}O$ values (Table S5) measured in the Diana metasyenite at Harrisville indicating significant interaction between the syenitic magma and the surrounding metasedimentary rocks. Vein titanite formed later than wallrock titanite and under different conditions. One such cm-scale vein titanite dated by U-Pb TIMS yielded a range of dates (1073–1016 Ma) that were interpreted to reflect crystallization during the Ottawan (Heumann, 2004). Vein mineralogy, especially the presence of calcite and calcsilicate minerals, indicates that vein fluids interacted with nearby metasedimentary rocks, including the extensive marbles of the Adirondack Lowlands located immediately to the NW (Fig. 1b,c). In addition, porphyroclastic grains with irregular rims (some T2 & T3) and dominantly porphyroblastic grains (T4) are consistent with metamorphic titanite growth. Accordingly, we characterize the chemical variation in the Harrisville titanite in order to constrain the relations between grain growth and oxygen isotope composition.

Titanite crystal chemistry and phase equilibria

Titanite is a monoclinic solid solution than can be broadly represented as (Ca, U, Pb, Mn, Th, REE)(Ti, Al, Fe, Zr, Ta, Nb, Y) [SiO_4] (O, F, OH) (Higgins & Ribbe, 1976; Tiepolo *et al.*, 2002; Mazdab, 2009). The *P-T* conditions of titanite stability are strongly dependent on bulk rock composition (e.g., Frost *et al.*, 2000). Theoretical (Wones, 1989; Xirouchakis *et al.*, 2001b), experimental (Xirouchakis *et al.*, 1998), and empirical (Xirouchakis *et al.*, 2001a; Harlov *et al.*, 2006) studies indicate that titanite stability in granitoid composition rocks is a function of temperature; pressure; f_{O_2}; α_{SiO_2}; and the activities of exchange vectors involving Fe^{2+}, Fe^{3+}, Ca^{2+}, and Ti^{4+}. Whether magmatic or metamorphic in origin, the persistence of titanite within the Diana metasyenite during upper amphibolite/granulite facies metamorphism was governed by the equilibria:

$$\begin{aligned}&\text{clinopyroxene/Ca-amphibole} + \text{ilmenite} + O_2 \\ &= \text{titanite} + \text{magnetite} + \text{quartz} \pm H_2O\end{aligned} \quad (1)$$

and

$$\text{rutile} + \text{calcite} + \text{quartz} = \text{titanite} + CO_2, \quad (2)$$

where clinopyroxene, Ca-amphibole, ilmenite, titanite and magnetite are solid solutions. Increasing oxygen fugacity drives the reaction 1 to the right (Xirouchakis *et al.*, 1998), and oxybarometry calculations by Cartwright *et al.* (1993) for the Harrisville outcrops are consistent with a titanite + magnetite + quartz assemblage close to the FMQ buffer at the temperatures and pressures of Ottawan metamorphism.

Element trends and zoning

The Harrisville titanite shows both intergrain (Fig. 4) and intragrain (Figs 5–8) variations in chemical composition. Aluminium, iron and fluorine are present at the level of minor elements in all studied titanite. High-field strength elements (Hf, Zr, Y) and rare earth elements (Ce & Nd) are present at trace levels and up to 1 element wt%. Intragrain zoning in major and minor elements is subtle with variations typically on the order of 0.2–0.5 element wt%, and rarely, up to 1 element wt% within a given grain. Zoning is most pronounced for Ti and elements that substitute on the ^{VI}Ti site (primarily Al and Fe^{3+}). Both electron microprobe traverses and electron backscatter imaging show that within a grain elemental zoning may be gradual, sharp or both.

To facilitate comparison and elucidate substitutional trends, titanite compositions are compared on the basis of formula atoms. T1 and T2 titanite grains are characterized by subtle differences in Al, Fe and F (Fig. 4); T1 grains generally have higher Ti and proportionally lower Al and Fe than T2 grains. T1 and T2 element profiles (Figs 5 & 6) are essentially flat with very small compositional variations within ~50 μm of grain edges. T3 vein titanite has distinctly higher (Al+F)/Fe ratios and, as a group, show the greatest compositional variability (Fig. 4). Vein titanite separates into two compositional subgroups (Type 3a and 3b in Fig. 4) that may reflect differences in vein emplacement sources or timing. Although all veins have similar mineralogy, the proportions of the minerals vary between veins. In addition, veins from which subgroup 3b titanite was sampled are commonly associated with potassic alteration. Compositional traverses across T3 grains (Fig. 7) also show greater intragrain compositional variation than T1 and T2 grains. T4 titanite is closest

to end-member composition and lowest in Al, Fe and F (Fig. 4); it shows essentially no compositional overlap with other titanite types. Compositional traverses across T4 grains (Fig. 8) show that subtle zoning occurs only near grain rims. Thus, the four microstructurally distinct populations of titanite are also chemically distinct, consistent with microstructural relations suggesting that these populations grew or recrystallized at different times and/or conditions.

TITANITE δ^{18}O ZONING

Figures 5–8 show SIMS δ^{18}O profiles from 13 titanite grains. For ease of discussion, each grain is designated by a number that indicates its type and order in the accompanying figure (e.g., T3.2 is the second Type-3 grain in Fig. 7). Note that throughout the descriptions below and the subsequent discussion, we distinguish δ^{18}O values, the VSMOW-standardized permil value, from δ^{18}O zoning, which refers to variations in δ^{18}O regardless of the VSMOW-standardized values. Because δ^{18}O variations rather than δ^{18}O values are of primary interest in this study, the error bars on δ^{18}O profile plots (and 2SD errors reported in Table S2) represent the *precision* of each measurement as calculated from the precision of the UWQ-1 quartz standard δ^{18}O measurements bracketing each group of titanite analyses; they do not represent a statistically complete analysis of the *accuracy* of the calculated titanite δ^{18}O values

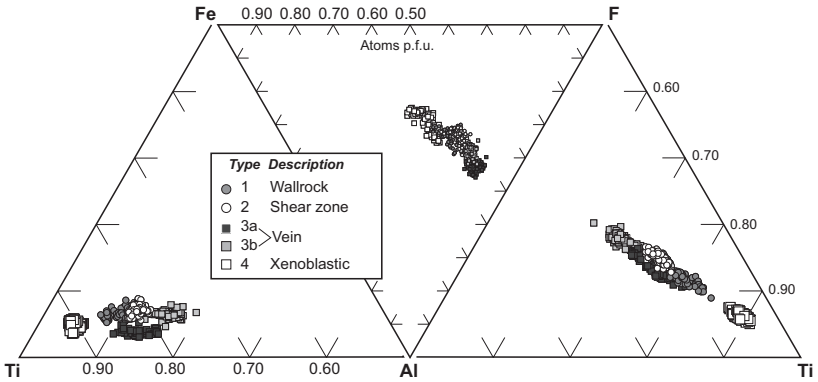

Fig. 4. Ternary plots showing titanite compositional variations in terms of atoms per formula unit titanium, iron, aluminium and fluorine. All analyses are plotted as a function of microstructurally determined titanite Type. T3 vein titanite is subdivided on the basis of compositional differences that may indicate two or more distinct vein emplacement episodes. Note that the scales on the right and left plots are expanded relative to the central plot.

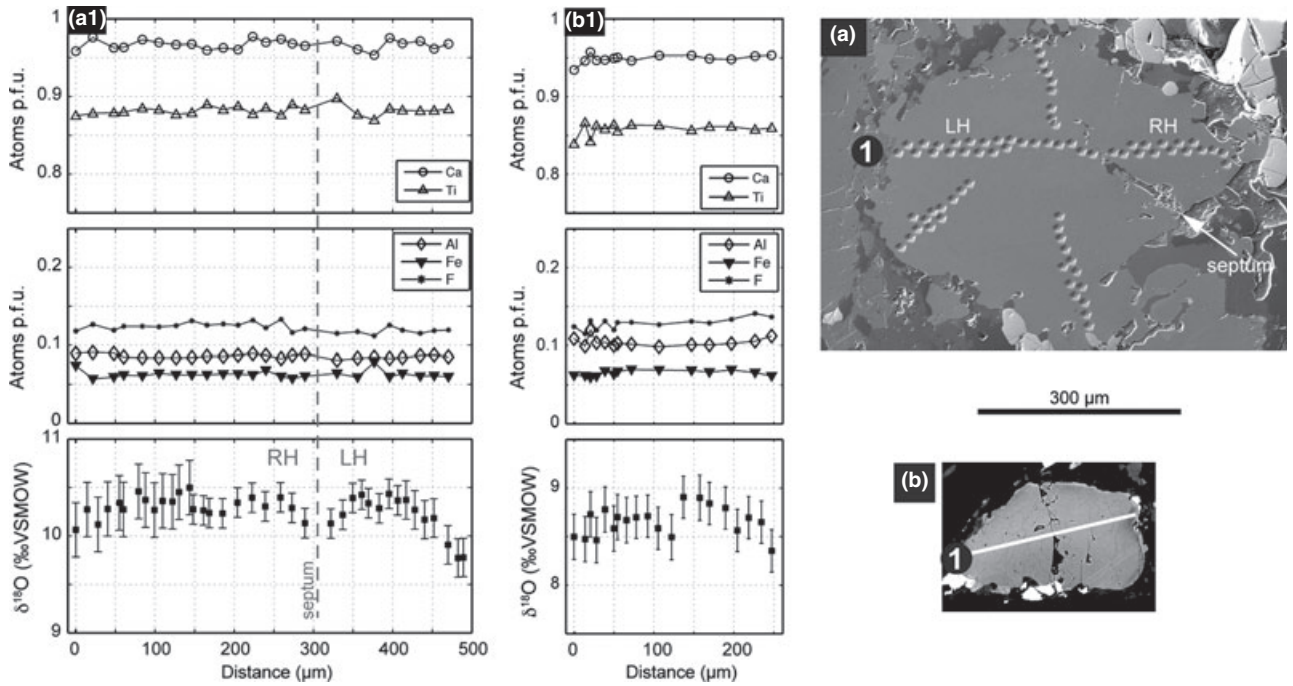

Fig. 5. Element and δ^{18}O zoning in Type-1 titanite grains. Traverse plots are keyed to grain images by letter and number. SIMS traverse paths are indicated on the grain images by white lines. On the images, the traverse number is placed at the origin of the traverse. (a) T1.1. Secondary electron image. A septum of included matrix minerals divides the grain into right-hand (RH) and left-hand domains (LH). (b) T1.2. BSE image with a narrowly focused contrast range.

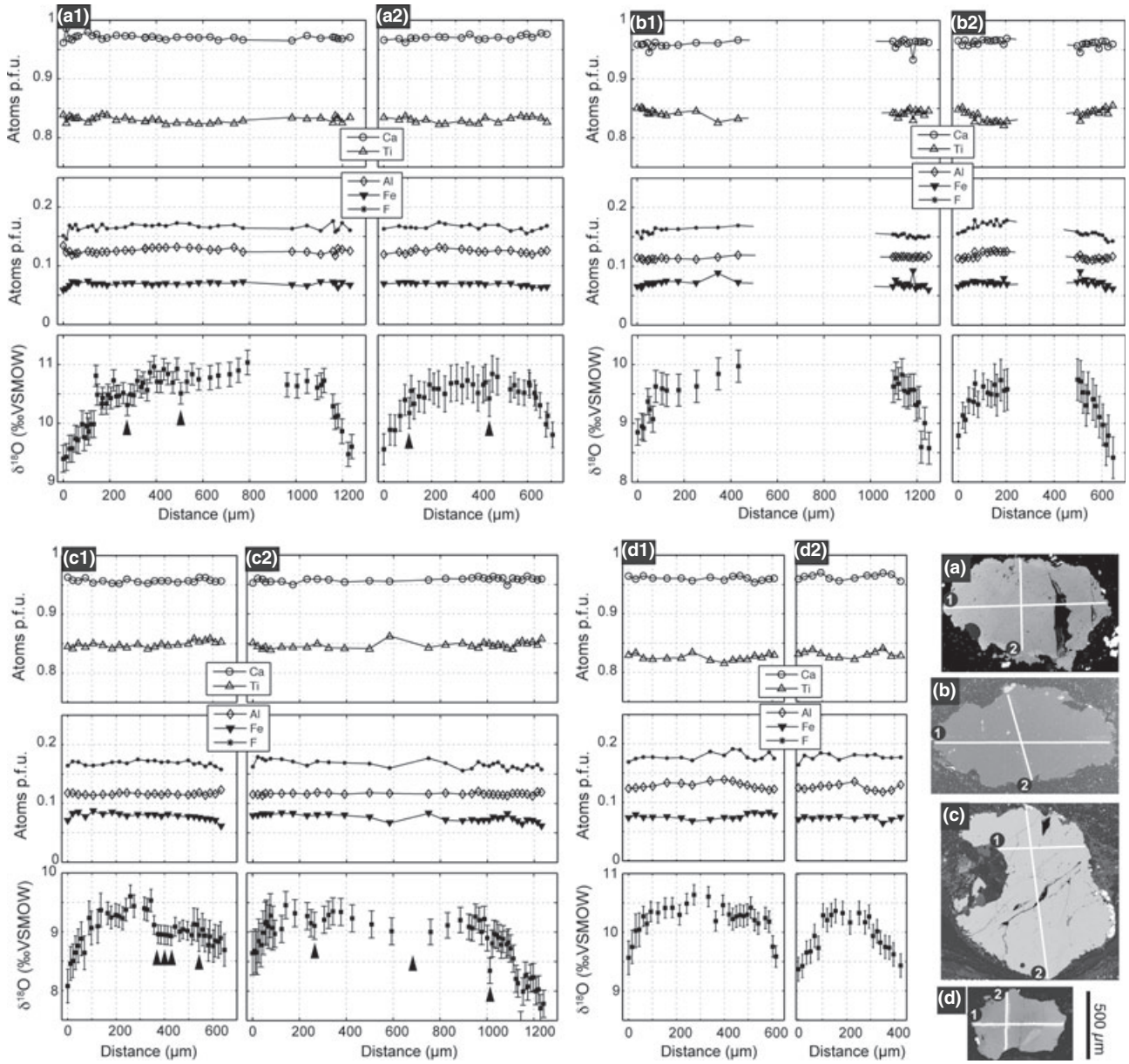

Fig. 6. Element and $\delta^{18}O$ zoning profiles in Type-2 titanite grains. Traverse plots are keyed to grain images by letter and number; there are multiple traverses per grain. SIMS traverse paths are shown on the grain images by white lines, and the traverse number is placed at the traverse origin. Arrows indicate places where SIMS traverses cross deformation twins. All grain images are BSE images except (b), which is a secondary electron image. (a) T2.1 (b) T2.2 (c) T2.3 (d) T2.4.

because errors on the bias correction curves have not been propagated.

The shapes, the average $\delta^{18}O$ values, and the $\Delta^{18}O$ (core-rim) of $\delta^{18}O$ profiles vary depending on the microstructural context of the individual titanite grain. Profiles are grouped according to the four distinct microstructural occurrences identified and described above (Fig. 3). In general, grains with petrographic evidence for significant deformation-induced (dynamic) recrystallization were avoided during SIMS analyses in order to minimize the potential for truncated or overprinted $\delta^{18}O$ profiles; however, several of the analyzed grains show internal deformation features such as undulose extinction and twinning. The relations between these deformational features and SIMS $\delta^{18}O$ measurements are described and discussed in detail below.

Type 1: Pre-S_1 wallrock titanite (Eastern outcrop)

Most T1 wallrock titanite shows evidence of dynamic recrystallization and grain-size reduction, and thus we gathered only two SIMS $\delta^{18}O$ profiles on this type of titanite. Both analyzed T1 grains show undulose extinction. T1.2 (~150 × 250 μm) also contains sparse, thin

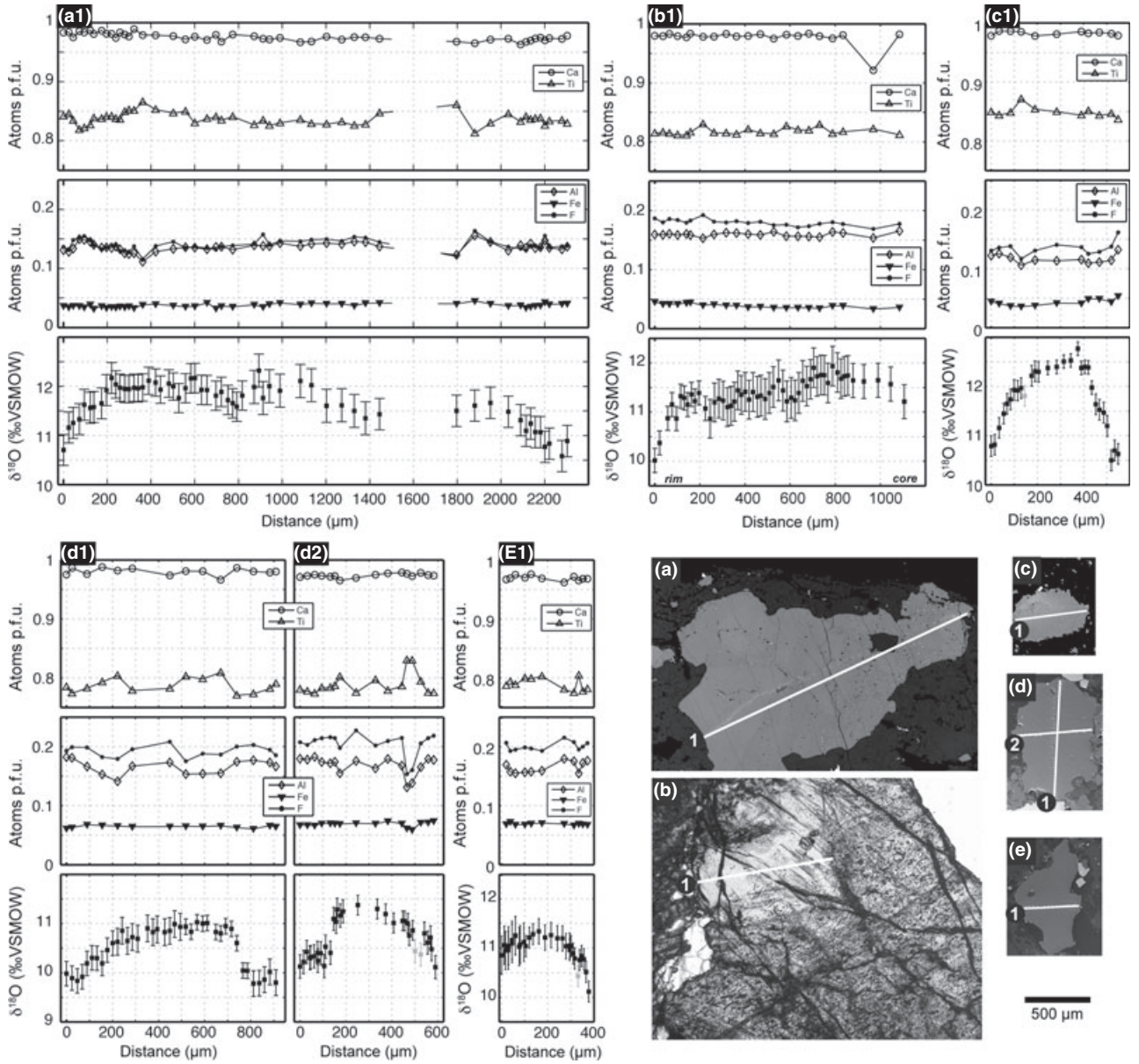

Fig. 7. Element and $\delta^{18}O$ zoning profiles in Type-3 titanite grains. Traverse plots are keyed to grain images by letter and number; there may be multiple traverses per grain. SIMS traverse paths are indicated on the grain images by white lines, and the traverse number is placed at the traverse origin. All grain images are BSE except (b), which is a plane-polarized transmitted light image. (a) T3.1 (b) T3.2 (c) T3.3 (d) T3.4 (e) T3.5.

lamellar twins and yields broadly core-to-rim decreasing $\delta^{18}O$ profile with $\Delta^{18}O$(core-rim) $\leq$0.4‰ (Fig. 5).

T1.1 (~300 × 500 μm), which lacks twin lamellae, yields a core-to-rim decreasing profile with $\Delta^{18}O$(core-rim) = 0.6‰ and is considered to be the best preserved T1 wallrock $\delta^{18}O$ profile (Fig. 5a). The oxygen isotope profile and crystallographic data for T1.1 were presented in detail in Bonamici *et al.* (2011) and are reviewed here as the best example of Type-1 titanite at Harrisville. Maximum $\delta^{18}O$ in the grain core is 10.4‰, which drops off steeply within 100 μm of the grain rim to 9.8‰. Electron backscatter diffraction (EBSD) mapping of this grain reveals two crystallographically distinct domains divided by a narrow septum of quartz and feldspar. The $\delta^{18}O$ values decrease toward the septum but the domains on either side retain approximately the same maximum $\delta^{18}O$ value of 10.4‰. Local misorientation mapping by EBSD of the left-hand crystallographic domain shows incipient subgrain boundary development that appears, at least in part, to correlate with small interior $\delta^{18}O$ fluctuations (Bonamici *et al.*, 2011).

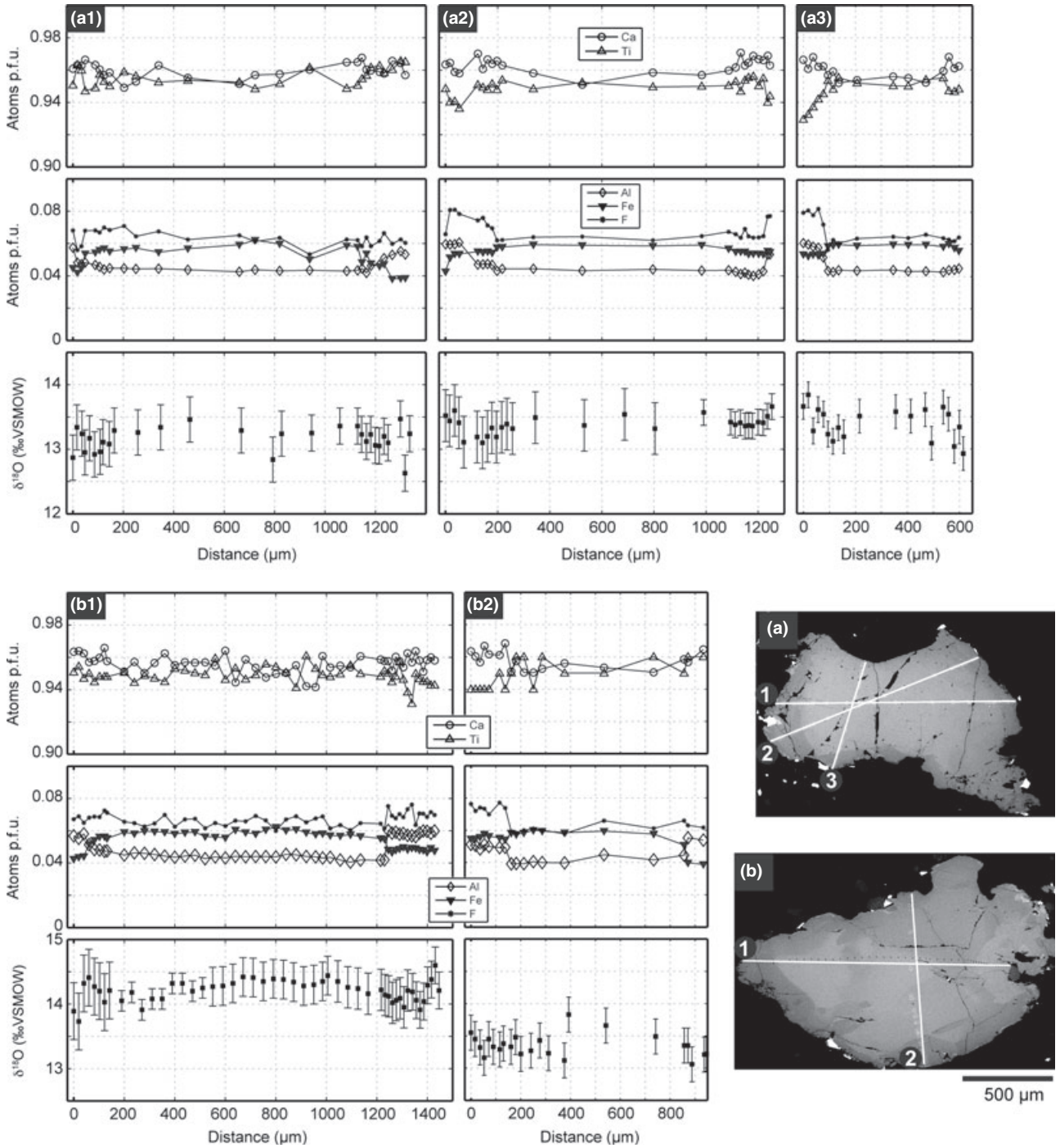

Fig. 8. Element and $\delta^{18}O$ zoning profiles in Type-4 titanite grains. Note that the formula atom range is expanded relative to Figs 5–7. Traverse plots are keyed to grain images by letter and number; there are multiple traverses per grain. SIMS traverse paths are indicated on the grain images by white lines, and the traverse number is placed at the traverse origin. Grain images are BSE with the contrast focused over a narrow band to enhance the chemical zoning. (a) T4.1 (b) T4.2.

Type 2: Pre/syn-S_2 shear-zone titanite (Eastern outcrop)

Oxygen isotope profiles from titanite in shear zones unassociated with vein material consistently show highest $\delta^{18}O$ values in grain cores decreasing smoothly and steeply to the lowest $\delta^{18}O$ values at the grain rims (Fig. 6). Maximum core $\delta^{18}O$ values are 9.7–10.8‰ and minimum $\delta^{18}O$ rim values are 7.7–9.6‰. Core-to-rim $\delta^{18}O$ differences are 1–1.5‰. T2 profiles are typically symmetric, with nearly identical $\delta^{18}O$ gradients and similar $\delta^{18}O$ values at either rim. T2.3 profiles show interior $\delta^{18}O$ fluctuations of

up to 0.5‰. As described above, T2.1 and T2.3 contain lamellar twins, which are usually visible in cross-polarized transmitted light as ~10–50 μm wide bands that either transect the grain entirely or disappear gradationally within the grain. Where SIMS traverses cross these twin bands, $\delta^{18}O$ decreases slightly but remains within analytical error of adjacent $\delta^{18}O$ values (arrows in Fig. 6).

Type 3: Syn-S_2 vein titanite (Eastern outcrop)

In general, vein titanite grains show first-order core-to-rim decreasing $\delta^{18}O$ values and $\Delta^{18}O$(core-rim) of 0.6–1.5‰ (Fig. 7); however, profiles from these grains also commonly display step-like $\delta^{18}O$ decreases and flat, lower-$\delta^{18}O$ rims (Fig. 7c–e). Values of $\delta^{18}O$ in T3 grains overlap with but are slightly elevated relative to $\delta^{18}O$ values in T1 and T2 grains. The lowest rim $\delta^{18}O$ values are 10‰ and the highest values in grain cores are 12‰. Most cm-scale vein titanite has undergone grain-size reduction by dynamic recrystallization. Only T3.2 lacks evidence of dynamic recrystallization, and it yields a $\delta^{18}O$ profile similar to T1 and T2 profiles (Fig. 7b1). Some millimetre-scale T3 titanite grains have asymmetric $\delta^{18}O$ profiles where one side of the profile shows a core-to-rim $\delta^{18}O$ gradient comparable to those in T1-2 grains and the other side is apparently truncated at higher $\delta^{18}O$ values. The truncated portion of the profile may be either directly at the grain boundary (Fig. 7e1) or adjacent to step-like $\delta^{18}O$ decrease and flattened, lower-$\delta^{18}O$ rim (Fig. 7d2). Some grain profiles have symmetrical flat $\delta^{18}O$ rims (Fig. 7c1,d1).

Type 4: Post-S_3 xenoblastic titanite (Western outcrop)

Values of $\delta^{18}O$ in T4 titanite range from 12.6 to 14.7‰, and are significantly higher than in other types of titanite (Fig. 8). The most significant zoning feature is a subtle increase in $\delta^{18}O$ toward the grain rims. Rim $\delta^{18}O$ zoning correlates spatially with chemical zoning apparent in compositional traverses (Fig. 8). Grain interiors are characterized either by essentially uniform $\delta^{18}O$ or by gradually decreasing $\delta^{18}O$. The $\delta^{18}O$ profile across T4.1 (Fig. 8a3) shows increasing $\delta^{18}O$ at one rim, where chemical zoning is well developed, but shows steeply decreasing $\delta^{18}O$ at the other rim, where the titanite grain abuts an augite grain and lacks sharp chemical zoning.

DISCUSSION

$\delta^{18}O$ zoning mechanisms: metamorphic growth *v.* diffusion *v.* recrystallization

Isotope exchange, like chemical exchange, among solid phases occurs by diffusion and recrystallization, both of which may or may not be fluid-mediated. Oxygen isotope exchange is a one-to-one trade of chemically (electronically) identical species with the same ionic radius that does not alter the total concentration of that species in the exchanging minerals (e.g., Zhang, 2010). It therefore differs from chemical/elemental exchange in that it does not require complex coupled substitutions that depend on the abundance of other elements, differential rates of exchange flux, maintenance of charge balance, size differences between exchanging elements, or net volume change of phases (e.g., Cole & Chakraborty, 2001). Consequently, rates of isotope exchange are more directly a function of the physical characteristics of exchange pathways, including their length, than are rates of cation exchange.

Harrisville titanite preserves broadly three kinds of $\delta^{18}O$ zoning profiles – (i) symmetric core-to-rim decreasing $\delta^{18}O$, (ii) asymmetric core-to-rim decreasing $\delta^{18}O$ with variable rim features and $\delta^{18}O$ gradients, and (iii) uniform interior $\delta^{18}O$ with slightly increasing $\delta^{18}O$ rims. This variety suggests that oxygen isotope zoning reflects more than one process or event. We compare microstructural observations, SIMS $\delta^{18}O$ profiles, and EPMA compositional data in order to distinguish between diffusion-, growth- and recrystallization-related zoning at different times in the history of the Harrisville titanite grains.

Profiles characterized by higher $\delta^{18}O$ in grain cores and steep, symmetrically decreasing $\delta^{18}O$ gradients at the grain rims (Figs 5 & 6) are consistent with diffusive exchange of oxygen during cooling from high-temperature (granulite) conditions. Cooling increases the magnitude of oxygen isotope fractionation between phases and should therefore decrease the $\delta^{18}O$ of weakly ^{18}O-partitioning minerals like titanite through exchange with modally dominant, strongly ^{18}O-partitioning minerals like quartz and feldspar. Although $\delta^{18}O$ values vary from grain to grain, all symmetrically decreasing $\delta^{18}O$ profiles exhibit similar 90% exchange distances (100 ± 20 μm) and similar $\delta^{18}O$ gradients at the grain rims (Fig. 9). Mineral growth is unlikely to produce such uniform and symmetric $\delta^{18}O$ gradients, especially over the range of grain sizes represented in the Harrisville data set (traverse lengths of ~400 μm to 1200 cm). Comparison of $\delta^{18}O$ zoning with element-zoning profiles (Figs 5 & 6) especially profiles of relatively immobile elements Ti and Al, reveals no correlation between the two. Decoupling of prograde element zoning and $\delta^{18}O$ zoning indicates that $\delta^{18}O$ zoning did not form in response to changing P–T–X conditions during growth.

Furthermore, symmetric core-to-rim decreasing $\delta^{18}O$ profiles occur in pre- or syn-S_2 grains with predominantly porphyroclastic microstructures (T1, T2, some T3). Smaller, grain-interior $\delta^{18}O$ variations superimposed on the grain-scale decreasing-$\delta^{18}O$ profiles correlate spatially with domains of intracrystalline deformation (Figs 5, 6b & 7a). T3.1 demonstrates the range of second-order $\delta^{18}O$ zoning features associ-

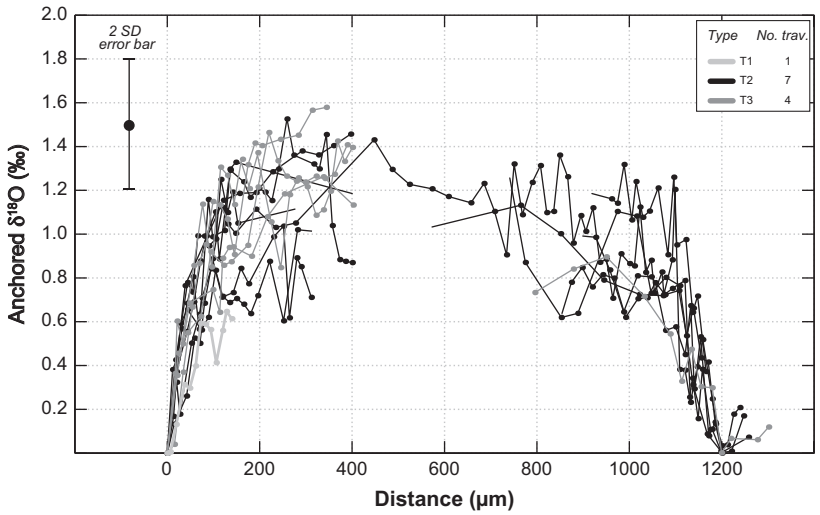

Fig. 9. $\delta^{18}O$ profiles for Types 1–3 titanite with core-to-rim $\delta^{18}O$ gradients (11 profiles from nine grains from six samples) anchored at zero permil to facilitate comparison and demonstrate the overall similarity of $\delta^{18}O$ profile shapes. The similarity of the $\delta^{18}O$ gradients is consistent with their formation by oxygen diffusion. Note that the complete profiles have different total lengths and rim $\delta^{18}O$ values. The number of traverses from each grain Type is indicated in the legend. Traverses are plotted from each grain boundary; apparent gaps in the middle of traverses are not real. Three profiles from Type 3 grains appear only on the left side of the figure either because their profiles were truncated by post-diffusion grain-shape modification (T3.3, T3.4) or because of an incomplete rim-to-rim analytical traverse (T3.2). See Figs 5-8 for the complete profiles.

ated with intracrystalline deformation in the Harrisville grains (Fig. 10). These include symmetrically decreasing $\delta^{18}O$ about subgrain boundaries, small (within analytical error) $\delta^{18}O$ fluctuations in the vicinity of lamellar twins, and bulk lowering of $\delta^{18}O$ values in partially recrystallized domains. The correlated occurrence of lower $\delta^{18}O$ and domains of intracrystalline deformation suggests that organized defects acted as pathways of increased diffusivity within titanite grains undergoing diffusive oxygen exchange.

Titanite grains with asymmetric core-to-rim decreasing $\delta^{18}O$ profiles (T2.3 and most T3 grains) reflect a combination of diffusion and recrystallization. While such grains show $\Delta^{18}O$(core-rim) ~0.5–1.5‰ comparable to diffusion-dominated grains, their $\delta^{18}O$ profiles also have variable-width rims of uniform or slightly increasing $\delta^{18}O$ (i.e., 'plateaus'), step-like $\delta^{18}O$ decreases, asymmetric $\delta^{18}O$ gradients, and/or asymmetric rim $\delta^{18}O$ values. These rim features are consistent with grain-shape modification by deformation-induced and/or dissolution-reprecipitation recrystallization. In some profiles, $\delta^{18}O$ gradients occurring inboard of flat $\delta^{18}O$ rim plateaus are identical to $\delta^{18}O$ gradients at the grain rims in symmetrically zoned grains (Fig. 7c), and thus some asymmetrically zoned grains may preserve intact diffusional zoning profiles toward the interior of the grain away from the current grain rims. On the other hand, where present, nearly vertical $\delta^{18}O$ steps and rim plateaus show no evidence of diffusive relaxation (Fig. 7c,d), indicating that recrystallization occurred at temperatures below blocking temperature for oxygen in titanite. Thus, asymmetrically $\delta^{18}O$ zoned grains with complex rims retain evidence for oxygen exchange at higher temperature followed by grain rim recrystallization at lower temperature.

Profiles characterized by uniform interior $\delta^{18}O$ and increasing $\delta^{18}O$ rims (T4; Fig. 8) primarily retain evidence for retrograde metamorphic growth zoning. Zoning of $\delta^{18}O$ occurs in the outer 100–400 μm of each grain and mimics major-minor element zoning, particularly zoning in Ti and Al (Fig. 8). Although the increasing-$\delta^{18}O$ rim zones appear in all profiles, the width of this zoning feature varies significantly between traverses, ranging from < 100 μm to >400 μm. Coupled isotopic-chemical zonation and variable-width rim zoning in T4 grains contrast with the decoupled isotopic and chemical zonation and constant-width rim zoning of diffusional profiles in T1 and T2 grains.

T4 grain interiors are unzoned in both $\delta^{18}O$ and chemical composition. We cannot therefore rule out the possibility of pre-existing diffusional profiles later modified by recrystallization and/or grain growth. In fact, one grain (T4.1) suggests that at least some T4 titanite contain inherited cores that once had diffusional profiles. T4.1 shares a margin with an augite crystal with two well-formed crystal faces that appear to have been shielded from recrystallization or later overgrowth by the titanite grain (Figs 8a & 11). In BSE images (Fig. 8a), darker rim zoning in the titanite grain is discontinuous across the margin shared with the augite grain, which is in direct contact with the BSE higher-contrast titanite grain core. A traverse ending at the titanite-augite boundary shows decreasing $\delta^{18}O$ with $\Delta^{18}O$(core-rim) = 0.8‰ and no

chemical zoning. The other end of the profile, where the traverse passes through a chemically zoned rim and ends at the boundary between titanite and the grain-size reduced quartz + feldspar shear zone matrix, shows the characteristic T4 increasing $\delta^{18}O$ and coupled chemical zoning (Fig. 11). We conclude that the currently observed $\delta^{18}O$ zoning in T4 titanite reflects predominantly titanite grain growth, either overgrowths on preexisting, partially dissolved cores or wholesale porphyroblast growth following S_3 shearing. The preservation of growth zoning implies that, unlike grains with symmetric core-to-rim decreasing $\delta^{18}O$, significant portions of T4 titanite, if not whole grains, grew at temperatures below the blocking temperature for oxygen.

In summary, the various $\delta^{18}O$ zoning patterns in Harrisville titanite and their respective interpretations in terms of growth, diffusion, and recrystallization can be correlated with and predicted from grain microstructural context. Pre- to syn-S_2 porphyroclasts (T1, T2, a few T3) display smooth, steep, nearly symmetric $\delta^{18}O$ gradients that extend to the current grain rim. Late syn-S_2 vein titanite with transitional porphyroclastic-porphyroblastic microstructures (most T3) shows overall core-to-rim decreasing $\delta^{18}O$, $\delta^{18}O$ steps, and/or asymmetric, lower-$\delta^{18}O$ rim plateaus consistent with diffusive zoning partially overprinted by recrystallization-related zoning. Post-S_3 titanite (T4 only) yields growth-dominated $\delta^{18}O$ zoning that correlates with chemical zoning.

Unifying time-temperature interpretation

The relative chronology of the microstructurally and chemically distinct titanite populations and the correlation of microstructure with $\delta^{18}O$ profile shape allows us to interpret the time-temperature development of oxygen isotope zoning in the Harrisville titanite (Fig. 12). We propose the following sequential development of the different titanite types and oxygen isotope zoning within them.

T1 and T2 titanite grains formed prior to the Ottawan tectonic phase and experienced the entirety of Ottawan metamorphism; their symmetrically decreasing $\delta^{18}O$ profiles record diffusive exchange during cooling from peak granulite-facies conditions. Core $\delta^{18}O$ values reflect high-temperature equilibrium with the surrounding metasyenite wallrock. Any prograde $\delta^{18}O$ growth zoning that existed in the T1 and T2 grains was erased by diffusive

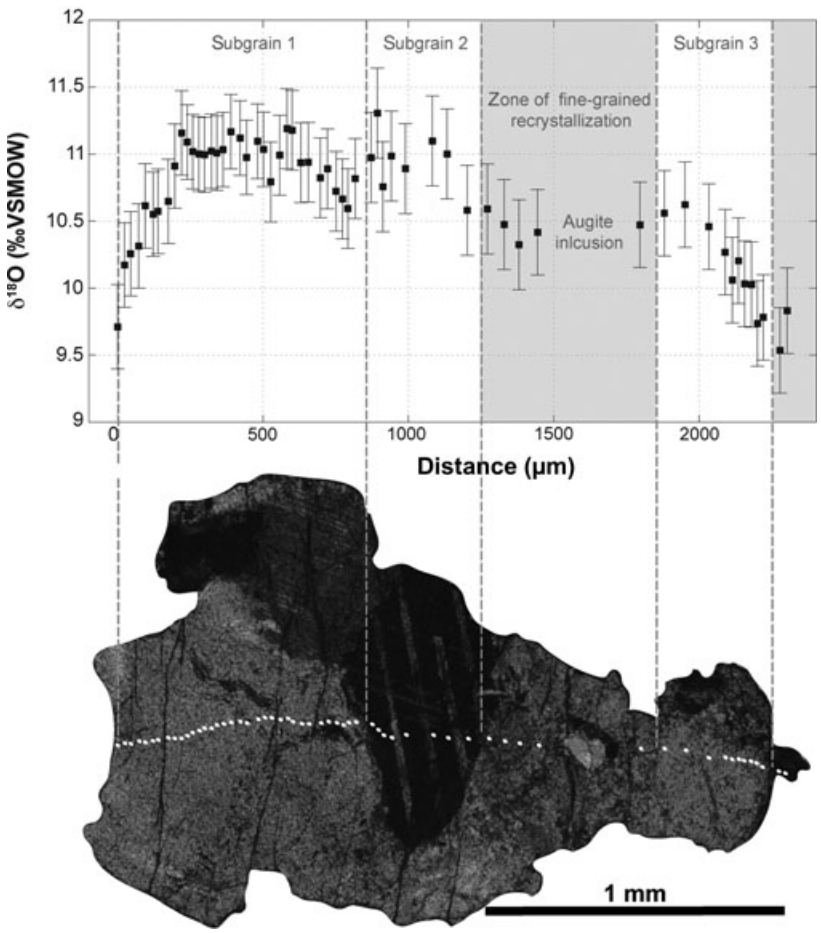

Fig. 10. Cross-polarized transmitted light photomicrograph of titanite grain T3.1 scaled to a plot of its $\delta^{18}O$ profile. See text for discussion. Grain-interior zoning is unusually well-developed in this example; grain-interior $\delta^{18}O$ fluctuations are typically much smaller and often within analytical error. SIMS analysis pits are indicated by small white dots. Subgrain boundaries are indicated by dashed marker lines.

exchange of oxygen at peak Ottawan conditions. Minor interior $\delta^{18}O$ zoning features in T1 and T2 grains reflect enhanced diffusivity along deformation-related intracrystalline defects, which must have formed either before or during Ottawan metamorphism. Thus, T1 and T2 $\delta^{18}O$ zoning profiles preserve a record of cooling from high-T conditions through the blocking temperature for oxygen.

T3 titanite $\delta^{18}O$ profiles record vein emplacement and development of the S_2 shear zone network during and shortly following peak *c.* 1050 Ma Ottawan metamorphism. Elevated $\delta^{18}O$ core values indicate that T3 grains grew initially in the presence of elevated-$\delta^{18}O$ fluids, which presumably infiltrated along S_2 shear zones and coeval with augite-rich veins. During post-peak cooling, many T3 grains developed core-to-rim decreasing, diffusion-dominated $\delta^{18}O$ profiles, which are still preserved in weakly deformed grains (Fig. 7a,b); however, most T3 grains were partially recrystallized at temperatures below the blocking temperature for oxygen as evidenced by abrupt (unrelaxed) $\delta^{18}O$ steps and $\delta^{18}O$ rim plateaus.

T4 titanite $\delta^{18}O$ zoning developed latest and at the lowest temperatures. Although T4 titanite cores may have formed earlier and at higher temperature, evidence of T2-style diffusive zoning was removed by deformation and/or dissolution, and T4 rims overgrew cores below the oxygen blocking temperature. The higher overall $\delta^{18}O$ values of T4 grain cores likely reflects differences in initial bulk-rock composition as indicated by the greater abundance of quartz in the ultramylonitic shear zone from which these grains were sampled, whereas the higher $\delta^{18}O$ rims suggest growth in the presence of an elevated-$\delta^{18}O$ fluid.

Oxygen isotope geospeedometry

Having distinguished diffusion-related zoning from other forms of zoning, it is possible to identify $\delta^{18}O$ profiles or portions of $\delta^{18}O$ profiles that are appropriate for diffusional modelling in order to quantify cooling rates in the Harrisville samples.

Diffusion modelling

Grain boundaries are generally 'fast' diffusion pathways along which oxygen diffusion is orders of magnitude faster than diffusion through crystal lattices (e.g., Manning, 1974; Eiler *et al.*, 1992, 1993; Valley, 2001; Watson & Baxter, 2007). Grain boundary diffusivity is a function of vacancy density (generally high), preferential impurity enrichment, and the presence or absence of fluids (Harrison, 1961). The Fast Grain Boundary (FGB) diffusion model proposes that under high-temperature conditions isotopic equilibrium is established and maintained along grain boundaries by rapid grain boundary diffusion (Eiler *et al.*, 1992). The FGB model has proven a successful tool for modelling the effects of *inter*grain oxygen diffusion on *intra*-grain oxygen isotope zoning in high-temperature systems (Eiler *et al.*, 1995a).

Eleven diffusion profiles from nine Harrisville titanite grains were modelled with an updated version of the FGB program (Eiler *et al.*, 1994), a one-dimensional numerical finite difference code that quantitatively implements the Fast Grain Boundary model. The FGB program fixes equilibrium at grain boundaries, balances the oxygen isotope flux between phases as each mineral grain exchanges internally by volume diffusion during cooling, and calculates the

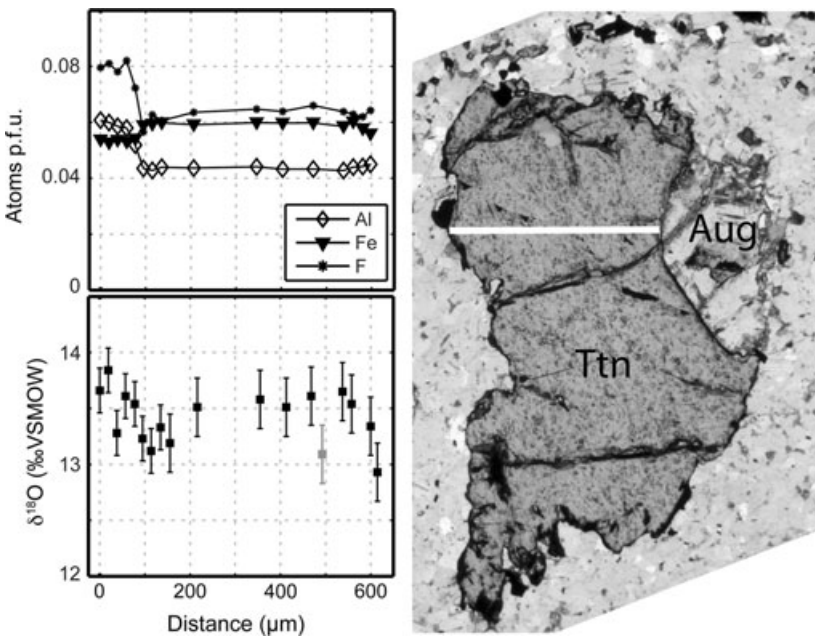

Fig. 11. Details of titanite grain T4.2 microstructure in relation to $\delta^{18}O$ and chemical zoning. Left side of the traverse shows typical Type 4 growth-dominated zoning, but the right side shows decreasing $\delta^{18}O$ toward the interface between titanite and the adjacent euhedral augite crystal face. Chemical and $\delta^{18}O$ zoning are decoupled on the right hand side of the traverse, typical of diffusion-dominated profiles.

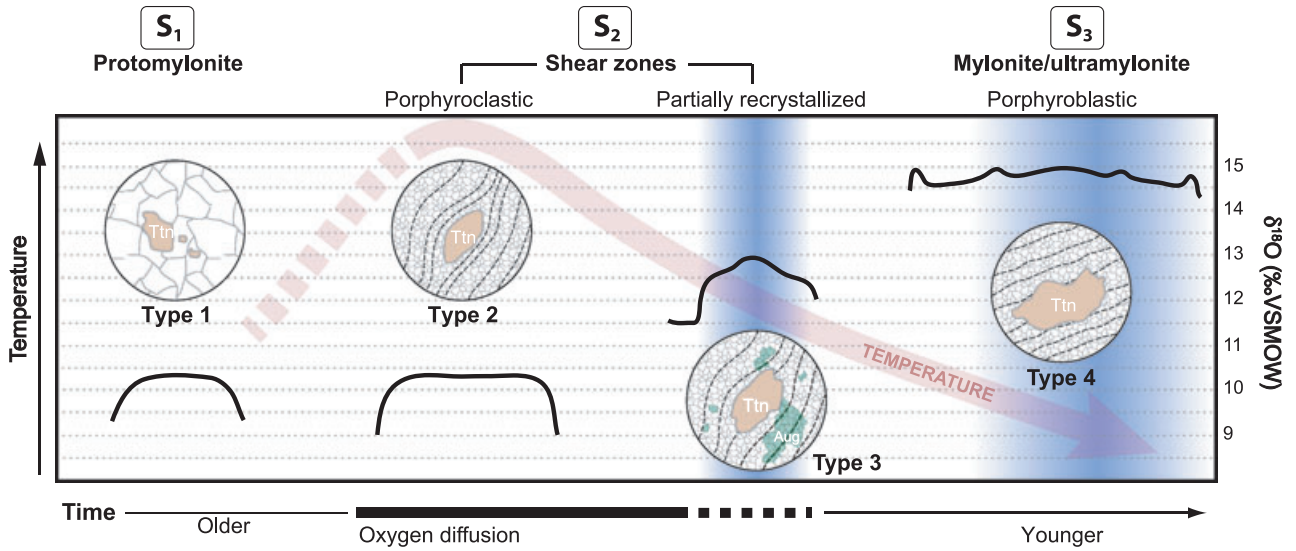

Fig. 12. Cartoon summary of the microstructures and relative time-temperature-fluid history along the Harrisville segment of the Carthage-Colton mylonite zone interpreted from $\delta^{18}O$ zoning in titanite. Arrow shows the temperature path relative to zoning profile development and fabric development. Type-1 and Type-2 titanite grains formed prior to peak-*T*, and their $\delta^{18}O$ profiles reflect diffusive oxygen exchange during and following peak-*T* conditions. Type-3 titanite formed during cooling and their $\delta^{18}O$ profiles reflect a combination of open- and closed-system (w.r.t. oxygen) zoning processes. Type-4 titanite $\delta^{18}O$ zoning profiles reflect predominantly closed-system, sub-blocking-*T* metamorphic growth. Vertical gradients schematically represent multiple, post-peak high-$\delta^{18}O$ fluid infiltration events.

time-integrated concentration profile in each phase within the modelled rock. In this study, only titanite profiles with diffusional $\delta^{18}O$ zoning were modelled and thus the majority of the models are for T1 and T2 grains (Figs 5 & 6); however, we also modelled four T3 profiles that show decreasing $\delta^{18}O$ gradients with $\Delta^{18}O$ (core-rim) $\geq 1‰$ that extend directly to the current grain rim (Fig. 7a1,b1,c1,d2). As discussed above, these T3 profiles are consistent with arrested-diffusion zoning preserved in unrecrystallized T3 grains or unrecrystallized portions of T3 grains. The profile for T1.2 was not modelled because microstructural evidence of partial dynamic recrystallization (twinning and well-developed undulose extinction) suggests significant $\delta^{18}O$ resetting by grain-interior fast-path diffusion, rather than volume diffusion.

Model results for the Harrisville titanite grains are shown in Fig. 13 and modelling parameters for each grain are listed in Appendix S1. Profile shapes are a function both of intrinsic parameters – modal mineralogy, grain size and shape, whole-rock $\delta^{18}O$, and titanite $\delta^{18}O$ (where titanite is not initially in equilibrium with the whole rock) – and extrinsic parameters – peak (starting) temperature, ending temperature, and cooling rate. Modelling generates intragrain $\delta^{18}O$ profiles for all phases in the model rock, but only titanite profiles will be discussed in detail here.

Intrinsic model parameters were constrained by, or inferred from, direct observation of the Harrisville samples. All models included quartz, alkali feldspar, clinopyroxene and titanite. Partial alteration of augite to amphibole, differences in wallrock and shear zone $\delta^{18}O$ values (Cartwright *et al.*, 1993; Table S5) and veins demonstrate the presence, at least locally, of hydrous fluids during post-peak metamorphic cooling and suggest that water fugacity was an important determinant of oxygen diffusivity (Edwards & Valley, 1998). Accordingly, models were constructed using experimental oxygen diffusivities for 'wet', or high-water-fugacity, conditions. Experimental oxygen diffusion data are not available for scapolite, which appears at up to 10 modal% in some vein-bearing samples; however, because of its compositional similarity to feldspar, scapolite was modelled in vein-bearing samples by increasing the feldspar modal percentage. Modal percentages were determined at the thin-section scale assuming that the mobility of oxygen along grain boundaries was sufficient for cm-scale transport (Eiler *et al.*, 1995a). Average grain sizes were measured on SEM images and photomicrographs. The grain size of a mineral can vary by 1–2 orders of magnitude within a sample; however, the models are relatively insensitive to the selected grain sizes of quartz, feldspar and clinopyroxene because of the large difference in modal abundances and diffusivities between these phases. Low oxygen diffusivity in clinopyroxene at model temperatures – slower than titanite – combined with its typically low modal abundance (~3–8%), limits its effect on ^{18}O mass balance during oxygen exchange with other phases in the model rock. Thus, titanite effectively exchanges only with quartz and feldspar, which have

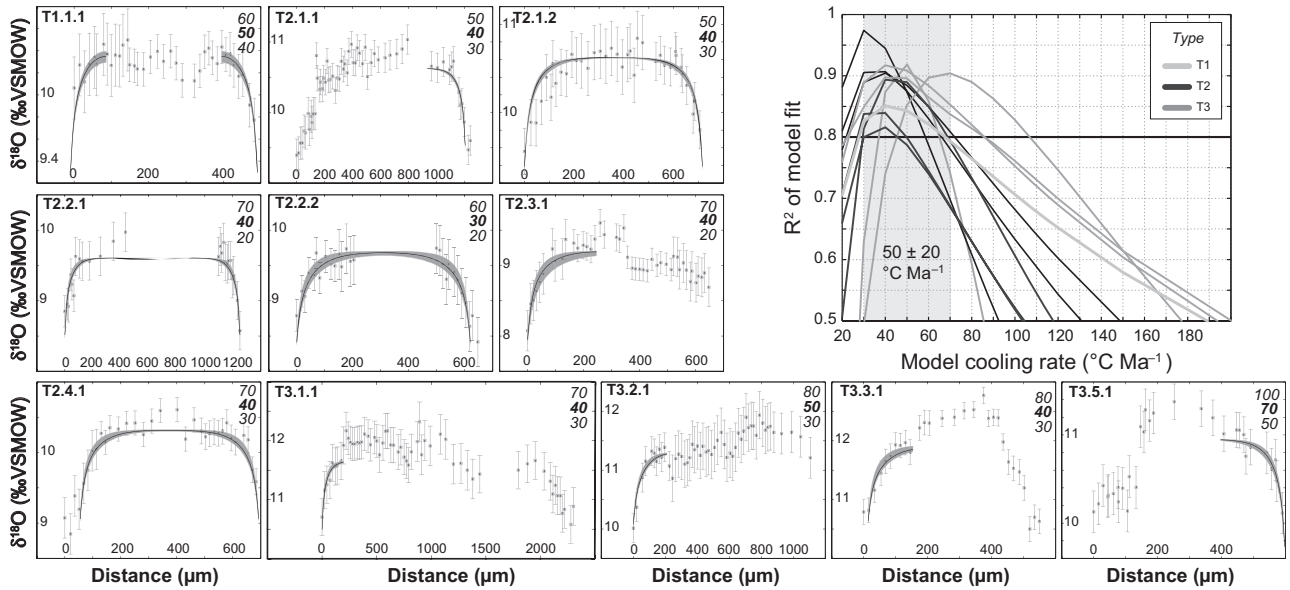

Fig. 13. Fast Grain Boundary modelling results for diffusion Harrisville titanite $\delta^{18}O$ diffusion profiles. Modelled temperature range is for cooling over the temperature range 675–500 °C for all grains. Gray envelope in each plot is defined by the slowest and fastest cooling rate models that give $R^2 \geq 0.8$. Slowest, fastest, best-fit (black line) cooling rates are also listed in the upper right-hand corner of each plot (best-fit in bold). The upper right-hand corner plot shows R^2 as a function of cooling rate for all models; all other fitting parameters are held constant. Note the convergence of best-fit R^2 values at 50 ± 20 °C Ma^{-1}.

such high oxygen diffusivities over the modelled temperature range that characteristic volume diffusion distances surpass the largest observed grain sizes for these minerals. All modelled grain profiles, except T1.1, show a flattened, approximately uniform $\delta^{18}O$ core that transitions through distinct, if slightly rounded, 'shoulders' to a steep $\delta^{18}O$ rim gradient. This profile morphology suggests that core $\delta^{18}O$ values represent the peak-temperature, pre-cooling $\delta^{18}O$ composition of the grain. Assuming oxygen isotope equilibrium between the titanite grain and the whole-rock at peak metamorphic conditions, the core $\delta^{18}O$ values were used to fix the initial equilibrium whole-rock $\delta^{18}O$ of the rock. To achieve the core-to-rim $\delta^{18}O$ difference observed in grain T3.2 (Fig. 7b1), the grain core composition was fixed at 11.3‰ while the whole-rock $\delta^{18}O$ was set at 0.2‰ lower than the equilibrium value – i.e., a very small initial disequilibrium was introduced to the model.

Extrinsic model parameters were constrained by data from regional and local studies of Ottawan metamorphic conditions. Phase equilibria (Bohlen *et al.*, 1985; Cartwright *et al.*, 1993) and carbon isotope thermometry (Gerdes & Valley, 1994; Kitchen & Valley, 1995) constrain peak Ottawan metamorphic temperatures in the Harrisville area at 650–700 °C, thus models were run for starting temperatures of 700, 675 and 650 °C. In general, profile shapes were best matched using a starting temperature of 675 °C. Models were run initially with cooling rates of 1–5 °C Ma^{-1} in accordance with the thermochronology studies of Mezger *et al.* (1991a, 1992) and Streepey *et al.* (2000, 2001), but when models employing these values yielded poor fits to the observed $\delta^{18}O$ profiles, the cooling rates were adjusted as the sole tuning variable to improve the model fits (Bonamici *et al.*, 2011).

RESULTS

Cooling rates that yield acceptable model fits ($R^2 \geq 0.8$) for the Harrisville $\delta^{18}O$ profiles fall between 20- and 160 °C Ma^{-1} (Fig. 13). Each modelled profile is compatible with a range of cooling rates that spans several tens of degrees per million years; however, all profiles have acceptable fits that fall within the range of 30–70 °C Ma^{-1}. We therefore consider this to be the most representative range of cooling rates for the Harrisville study area. In eight out of 12 models, observed $\delta^{18}O$ profiles are best fit by 40 °C Ma^{-1} cooling rate.

Tectonic implications

Cooling rates determined from numerical modelling are consistently and significantly higher than cooling rates determined from multi-mineral thermochronology for the Adirondack region (Fig. 14). Cooling rates from oxygen diffusion profiles indicate a relatively short-lived (≤5 Ma) period of rapid cooling (this study; (Bonamici *et al.*, 2011), whereas the combined closure temperatures and ages of monazite, garnet, titanite, hornblende and rutile yield a time-averaged cooling rate of 1–5 °C Ma^{-1} for both the Adiron-

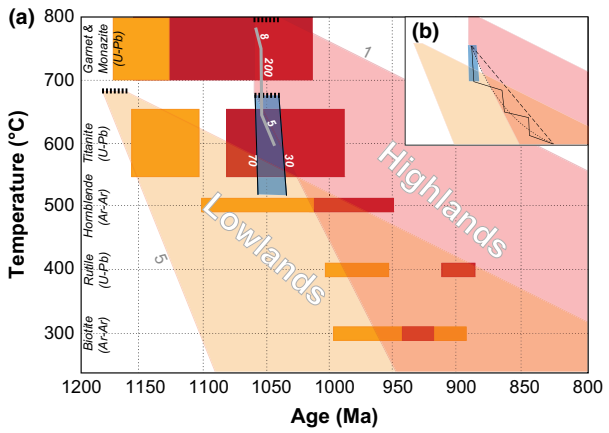

Fig. 14. (a) Temperature-time diagram showing all thermochronological data currently available for the northwestern Adirondack Highlands (darker grays) and the Adirondack Lowlands (lighter grays). Rectangles are bulk-mineral closure constraints from regional thermochronology studies, compiled from Mezger *et al.* (1991b, 1992); Streepey *et al.* (2000, 2001); Dahl *et al.* (2004); Storm & Spear (2005). Triangular domains are cooling envelopes originating at the temperature and age of peak metamorphism for each domain (dotted lines) and bounded by the slowest (1 °C Ma^{-1}) and fastest (5 °C Ma^{-1}) cooling rates proposed by Mezger *et al.* (1991a). Note that peak-*T* was lower at Harrisville (675–700 °C) than in the central Highlands (800 °C). Data from this study are shown by the black-outlined cooling envelope that originates at the peak temperature for the Harrisville site (675 °C) and is bounded by the upper (70 °C Ma^{-1}) and lower (30 °C Ma^{-1}) cooling rates determined from oxygen isotope diffusion modelling. Bold pale gray line defines a segmented cooling path proposed for the southern Adirondacks on the basis of by Fe-Mg zoning in garnet (Storm & Spear, 2005); for all linear cooling path segments, italicized numbers are cooling rates in °C Ma^{-1}. (b) Cartoon showing the Adirondack cooling envelopes relative to three schematic cooling paths (dashed and solid black lines) and their possible relations to thermochronological constraints – linear (steady state), $1/T$ (gradually varying), and stepwise. For the stepwise path, which is supported by diffusion modelling of titanite $\delta^{18}O$ profiles, steep path segments correlate to periods of rapid cooling following deformation, whereas gradual segments represent periods of limited deformation and slow, near-isobaric cooling. Figure modified from Bonamici *et al.* (2011) and additional data included.

dack Highlands and the Adirondack Lowlands over ~200 Ma (Mezger *et al.*, 1991a, 1993). This difference appears to be a significant discrepancy, but more likely it arises from the fundamentally different spatial and, thus, temporal resolutions of the two data sets. Oxygen isotope zoning in titanite preserves a high (temporal) resolution record of the thermal history of the Harrisville segment of the CCMZ; regional multi-mineral thermochronology provides a lower (temporal) resolution record of the regional Adirondack thermal history.

Bonamici *et al.* (2011) proposed that the mechanism of fast cooling was rapid exhumation and juxtaposition of the northwestern Adirondack Highlands against the structurally higher and cooler Adirondack Lowlands during or shortly following the peak of Ottawan metamorphism. The predominantly northwestward dip of CCMZ fabrics and local normal-sense shear indicators (Heyn, 1990) suggest that exhumation was the result of extension. Extension-related exhumation accords with previous conclusion that the CCMZ accommodated gravitational collapse of the Ottawan orogen (Mezger *et al.*, 1991b, 1992; Streepey *et al.*, 2001; Johnson *et al.*, 2004; Selleck *et al.*, 2005; Wong *et al.*, 2012).

In the context of a major crustal shear zone like the CCMZ (1–5 km wide by >100 km along strike), slip events accommodating large vertical displacement are likely to result in large thermal gradients that induce rapid cooling. In fact, shear zones that juxtapose crustal blocks with different temperatures should be the locus of the highest (local or regional) thermal gradients by definition, and thus rocks within and immediately adjacent to such shear zones should experience the highest rates of thermal diffusion and record the fastest cooling rates for a deforming system. Deformation-induced or -enhanced fluid infiltration is also likely to promote advective heat loss and focus rapid cooling along shear zones. Furthermore, most faults and, by extension, probably most shear zones, experience transient periods of active deformation separated by intervals of relative quiescence. Thus, punctuated, stepwise cooling histories should be the norm in the vicinity of such structures. However, the low thermal conductivity of most rocks (and especially mid-crustal rocks) is likely to result in attenuation of a punctuated thermal signal at a distance from the signal source (i.e., the shear zone). Consequently, slower, steadier cooling rates inferred from regional thermochronology studies in the Adirondack Mountains may, in part, reflect sampling far from strain localization features like major shear zones. We speculate that although the Adirondack Highlands as a whole experienced episodic exhumation during Ottawan gravitational collapse, only specific geological locations preserve a punctuated thermal history. This conclusion highlights one way in which sample location can complicate the quantification of exhumation or uplift rates from thermochronologic data.

Transient fluid infiltration

The combination of elevated overall $\delta^{18}O$ values and core-to-rim decreasing $\delta^{18}O$ zoning in T3 titanite grains (Fig. 7) pins the timing of S_2 shear zone development relative to the Harrisville cooling history. Elevated core $\delta^{18}O$ values (relative to pre-S_2 T1–2 grains) signal increased whole-rock $\delta^{18}O$ during T3 grain growth, likely by infiltration of high-$\delta^{18}O$ fluids in association with shear zone and vein formation. Indeed, most T3 grains contain aligned μm-scale voids indicative of growth in the presence of a fluid, and (Cartwright *et al.*, 1993) noted that fluids inter-

acting with abundant, nearby metasedimentary rocks (Fig. 1b,c) after the peak of metamorphism, though still at elevated temperatures, were likely to be enriched in ^{18}O. However, had high-$\delta^{18}O$ fluid infiltration continued throughout the time that titanite was yet open to oxygen diffusion, it is probable that the grain boundary oxygen reservoir with which titanite was exchanging would have become a source rather than a sink for ^{18}O, such that diffusive oxygen exchange would produce higher, not lower, $\delta^{18}O$ rims. Instead, the observed lower-$\delta^{18}O$ rims on T1, T2 and T3 grains indicate diffusive exchange during cooling in the absence of a high-$\delta^{18}O$ fluid. In addition, many T3 grains also have lower $\delta^{18}O$ rim plateaus indicating grain recrystallization or growth in the absence of an elevated-$\delta^{18}O$ fluid and below the partial-retention zone for oxygen. Thus, T3 titanite $\delta^{18}O$ profiles suggest that fluid infiltration occurred during active S_2 shearing and shut off when deformation ceased. This type of fluid 'pumping' is consistent with shear zone behaviours predicted (e.g., Sibson *et al*., 1975; McCaig, 1988) and inferred (e.g., Ingebritsen & Manning, 1999; 2010) for many active shear zone systems but has never before been extracted from a grain-scale geochemical record, and it hints at the potential of integrated (micro)structural-isotopic studies to tease out information about fine-scale deformation dynamics in ancient systems.

CONCLUSIONS

1 Subtle ($>0.3‰$) zoning in the oxygen isotope ratios of titanite can be reliably resolved at the 10-μm scale with SIMS.
2 Diana metasyenite and various crosscutting augite-rich veins host four microstructurally distinct populations of titanite, each of which has a different composition, major-minor element zoning pattern, and $\delta^{18}O$ zoning pattern. By careful comparison of microstructural and compositional data, it is possible to distinguish $\delta^{18}O$ zoning arising from diffusion, recrystallization, and growth.
3 Microstructurally constrained patterns of oxygen isotope zoning in titanite provide a detailed time-temperature-fluid history for the Harrisville segment of the Carthage-Colton mylonite zone in the Adirondack Mountains of New York. Elevated-$\delta^{18}O$ fluids infiltrated during active shearing and formation of the oblique-slip S_2 shear zones network at temperatures near the local peak of Ottawan metamorphism.
4 Fast Grain Boundary diffusion modelling of $\delta^{18}O$ zoning suggests relatively rapid cooling from the peak Ottawan metamorphism at ~675°C to 500°C in ≤5 Ma (cooling rates of 50 ± 20 °C Ma^{-1}), consistent with a period of rapid tectonic exhumation of the northwestern Adirondack Highlands along the CCMZ.
5 The diffusivity of oxygen in titanite and the improved precision of $\delta^{18}O$ measurements by the SIMS technique make titanite a useful monitor of high-temperature mass transfer processes at least up to lower-granulite facies conditions.

ACKNOWLEDGEMENTS

We thank N. Kita, J. Kern, K. Kitajima and A. Strickland for assistance in the WiscSIMS laboratory; J. Fournelle for assistance with EPMA analysis; and B. Hess for sample preparation. This research was funded by the NSF (EAR0838058), DOE (93ER14389), and GSA (student research grant 9224-10). CB was supported by the Kenneth & Linda Ciriacks Graduate Fellowship through the UW-Madison Department of Geoscience. WiscSIMS is partially supported by NSF-EAR (0319230, 0744079, 1053466).

REFERENCES

Abart, R. & Pozzorini, D., 2000. Implications of kinetically controlled mineral-fluid exchange on the geometry of stable-isotope fronts. *European Journal of Mineralogy*, **12,** 1069–1082.
Baird, G.B. & MacDonald, W., 2004. Deformation of the Diana syenite and Carthage-Colton mylonite zone: Implications for timing of Adirondack Lowlands deformation. *Geological Society of America Memoir*, **197,** 285–297.
Bohlen, S., Valley, J.W. & Essene, E., 1985. Metamorphism in the Adirondacks. I. Petrology, pressure and temperature. *Journal of Petrology*, **26,** 971–992.
Bonamici, C., Kozdon, R., Ushikubo, T. & Valley, J.W., 2011. High-resolution P-T-t paths from $\delta^{18}O$ zoning in titanite: A snapshot of late-orogenic collapse in the Grenville of New York. *Geology*, **39,** 959–962.
Bowman, J.R., Valley, J.W. & Kita, N.T., 2009. Mechanisms of oxygen isotopic exchange and isotopic evolution of $^{18}O/^{16}O$-depleted periclase zone marbles in the Alta aureole, Utah: Insights from ion microprobe analysis of calcite. *Contributions to Mineralogy and Petrology*, **157,** 77–93.
Cartwright, I., Valley, J.W. & Hazelwood, A.-M., 1993. Resetting of oxybarometers and oxygen isotope ratios in granulite facies orthogneisses during cooling and shearing, Adirondack Mountains, New York. *Contributions to Mineralogy and Petrology*, **113,** 208–225.
Chacko, T., Cole, D.R. & Horita, J., 2001. Equilibrium oxygen, hydrogen, and carbon isotope fractionation factors applicable to geologic systems. *Reviews in Mineralogy and Geochemistry*, **43,** 1–62.
Chappell, J., Bickford, M.E., Selleck, B.W., Wooden, J., Mazdab, F. & Heumann, M.J., 2006. High-temperature shearing and pegmatite formation during Ottawan extensional collapse, northwestern Adirondack Mountains, New York. *Geological Society of America Abstracts with Programs*, **38,** 385.
Cole, D. & Chakraborty, S., 2001. Rates and mechanisms of isotopic exchange. *Reviews in Mineralogy and Geochemistry*, **43,** 83–191.
Cole, D.R., Larson, P.B., Riciputi, L.R. & Mora, C.I., 2004. Oxygen isotope zoning profiles in hydrothermally altered feldspars: Estimating the duration of water-rock interaction. *Geology*, **32,** 29.
Dahl, P.S., Pomfrey, M.E. & Foland, K.A., 2004. Slow cooling and apparent tilting of the Adirondack Lowlands, Grenville

Province, New York, based on $^{40}Ar/^{39}Ar$ ages. *Geological Society of America Memoir*, **197,** 299–323.
D'Errico, M.E., Lackey, J.S., Surpless, B.E. *et al.* , 2012. A detailed record of shallow hydrothermal fluid flow in the Sierra Nevada magmatic arc from low-$\delta^{18}O$ skarn garnets. *Geology*, **40,** 763–766.
Donovan, J., Kremser, D. & Fournelle, J.H., 2009. *Probe for EPMA: Acquisition, Automation and Analysis*. Probe Software Inc., Eugene, Oregon.
Edwards, K. & Valley, J.W., 1998. Oxygen isotope diffusion and zoning in diopside: The importance of water fugacity during cooling. *Geochimica et Cosmochimica Acta*, **62,** 2265–2277.
Eiler, J.M., Baumgartner, L.P. & Valley, J.W., 1992. Intercrystalline stable isotope diffusion: A fast grain boundary model. *Contributions to Mineralogy and Petrology*, **112,** 543–557.
Eiler, J.M., Valley, J.W. & Baumgartner, L.P., 1993. A new look at stable isotope thermometry. *Geochimica et Cosmochimica Acta*, **57,** 2571–2583.
Eiler, J.M., Baumgartner, L.P. & Valley, J.W., 1994. Fast Grain Boundary: A Fortran-77 program for calculating the effects of retrograde interdiffusion of stable isotopes. *Computers & Geosciences*, **20,** 1415–1434.
Eiler, J.M., Valley, J.W., Graham, C. & Baumgartner, L.P., 1995a. Ion microprobe evidence for the mechanisms of stable isotope retrogression in high-grade metamorphic rocks. *Contributions to Mineralogy and Petrology*, **118,** 365–378.
Eiler, J.M., Valley, J.W., Graham, C.M. & Baumgartner, L.P., 1995b. The oxygen isotope anatomy of a slowly cooled metamorphic rock. *American Mineralogist*, **80,** 757–764.
Ferry, J.M., Ushikubo, T., Kita, N.T. & Valley, J.W., 2010. Assessment of grain-scale homogeneity and equilibration of carbon and oxygen isotope compositions of minerals in carbonate-bearing metamorphic rocks by ion microprobe. *Geochimica et Cosmochimica Acta*, **74,** 6517–6540.
Ferry, J.M., Ushikubo, T. & Valley, J.W., 2011. Formation of forsterite by silicification of dolomite during contact metamorphism. *Journal of Petrology*, **52,** 1619–1640.
Frost, B., Chamberlain, K. & Schumacher, J., 2000. Sphene (titanite): Phase relations and role as a geochronometer. *Chemical Geology*, **172,** 131–148.
Gerdes, M.L. & Valley, J.W., 1994. Fluid flow and mass transport at the Valentine wollastonite deposit, Adirondack Mountains, New York State. *Journal of Metamorphic Geology*, **12,** 589–608.
Gerdes, M., Baumgartner, L.P., Person, M. & Rumble, D., 1995. One-and two-dimensional models of fluid flow and stable isotope exchange at an outcrop in the Adamello contact aureole, Southern Alps, Italy. *American Mineralogist*, **80,** 1004–1019.
Hamilton, M., McLelland, J. & Selleck, B.W., 2004. SHRIMP U-Pb zircon geochronology of the anorthosite-mangerite-charnockite-granite suite, Adirondack Mountains, New York: Ages of emplacement and metamorphism. *Geological Society of America Memoir*, **197,** 337–356.
Harlov, D., Tropper, P., Seifert, W., Nijland, T. & Förster, H., 2006. Formation of Al-rich titanite ($CaTiSiO_4O$-$CaAlSiO_4OH$) reaction rims on ilmenite in metamorphic rocks as a function of f_{H2O} and f_{O2}. *Lithos*, **88,** 72–84.
Harrison, L., 1961. Influence of dislocations on diffusion kinetics in solids with particular reference to the alkali halides. *Transactions of the Faraday Society*, **57,** 1191–1199.
Harrison, T.M., Heizler, M.T., McKeegan, K.D. & Schmitt, A.K., 2010. In situ 40K–40Ca "double-plus" SIMS dating resolves Klokken feldspar 40K–40Ar paradox. *Earth and Planetary Science Letters*, **299,** 426–433.
Hartley, M.E., Thordarson, T., Taylor, C., Fitton, J.G. & EIMF, 2012. Evaluation of the effects of composition on instrumental mass fractionation during SIMS oxygen isotope analyses of glasses. *Chemical Geology*, **334,** 312–323.
Heumann, M.J., 2004. *Thermochronological and Geochronological studies in the Adirondack Highlands and Lowlands, New York*. MS thesis. Syracuse University, 118 pp.
Heyn, T., 1990. *Tectonites of the northwest Adirondack Mountains, New York: Structural and Metamorphic evolution*. PhD thesis. Cornell University, 230 pp.
Higgins, J. & Ribbe, P., 1976. The crystal chemistry and space groups of natural and synthetic titanites. *American Mineralogist*, **61,** 878–888.
Ingebritsen, S.E. & Manning, C.E., 1999. Geological implications of a permeability-depth curve for the continental crust. *Geology*, **27,** 1107–1110.
Ingebritsen, S.E. & Manning, C.E., 2010. Permeability of the continental crust: Dynamic variations inferred from seismicity and metamorphism. *Geofluids*, **10,** 193–205.
Johnson, E., Goergen, E. & Fruchey, B.L., 2004. Right lateral oblique slip movements followed by post-Ottawan (1050–1020 Ma) orogenic collapse along the Carthage-Colton shear zone: Data from the Dana Hill metagabbro body, Adirondack Mountains, New York. *Geological Society of America Memoir*, **197,** 357–378.
Kelly, J.L., Fu, B., Kita, N.T. & Valley, J.W., 2007. Optically continuous silcrete quartz cements of the St. Peter Sandstone: High precision oxygen isotope analysis by ion microprobe. *Geochimica et Cosmochimica Acta*, **71,** 3812–3832.
Kita, N.T., Ushikubo, T., Fu, B. & Valley, J.W., 2009. High precision SIMS oxygen isotope analysis and the effect of sample topography. *Chemical Geology*, **264,** 43–57.
Kitchen, N. & Valley, J.W., 1995. Carbon isotope thermometry in marbles of the Adirondack Mountains, New York. *Journal of Metamorphic Geology*, **13,** 577–594.
Kohn, M.J., Valley, J.W., Elsenheimer, D & Spicuzza, M.J., 1993. O isotope zoning in garnet and staurolite: Evidence for closed-system mineral growth during regional metamorphism. *American Mineralogist*, **78,** 988–1001.
Lackey, J.S. & Valley, J.W., 2004. Complex patterns of fluid flow during wollastonite formation in calcareous sandstones at Laurel Mountain, Mt. Morrison Pendant, California. *Geological Society of America Bulletin*, **116,** 76–93.
Manning, J.R., 1974. Diffusion kinetics and mechanisms in simple crystals. *Carnegie Institution of Washington Publication*, **634,** 3–13.
Mazdab, F., 2009. Characterization of flux-grown trace-element-doped titanite using high-mass-resolution ion microprobe (SHRIMP-RG). *Canadian Mineralogist*, **47,** 813–831.
McCaig, A.M., 1988. Deep fluid circulation in fault zones. *Geology*, **16,** 867.
McLelland, J. & Daly, J., 1996. The Grenville orogenic cycle (ca. 1350-1000 Ma): An Adirondack perspective. *Tectonophysics*, **265,** 1–28.
McLelland, J., Hamilton, M. & Selleck, B.W., 2001. Zircon U-Pb geochronology of the Ottawan orogeny, Adirondack highlands, New York: Regional and tectonic implications. *Precambrian Research*, **109,** 39–72.
Mezger, K., Rawnsley, C., Bohlen, S. & Hanson, G., 1991a. U-Pb garnet, sphene, monazite, and rutile ages: Implications for the duration of high-grade metamorphism and cooling histories, Adirondack Mts, New York. *The Journal of Geology*, **99,** 415–428.
Mezger, K., van der Pluijm, B., Essene, E. & Halliday, A., 1991b. Synorogenic collapse: A perspective from the middle crust, the Proterozoic Grenville Orogen. *Science*, **254,** 695–698.
Mezger, K., van der Pluijm, B., Essene, E. & Halliday, A., 1992. The Carthage-Colton Mylonite Zone (Adirondack Mountains, New York): The Site of a Cryptic Suture in the Grenville Orogen? *The Journal of Geology*, **100,** 630–638.
Mezger, K., Essene, E., van der Pluijm, B. & Halliday, A., 1993. U-Pb geochronology of the Grenville Orogen of Ontario and New York: Constraints on ancient crustal tec-

tonics. *Contributions to Mineralogy and Petrology*, **114,** 13–26.
Nabelek, P., 2002. Calc-silicate reactions and bedding-controlled isotopic exchange in the Notch Peak aureole, Utah: Implications for differential fluid fluxes with metamorphic grade. *Journal of Metamorphic Geology*, **20,** 429–440.
Peck, W.H., Valley, J.W. & Corriveau, L., 2004. Oxygen-isotope constraints on terrane boundaries and origin of 1.18–1.13 Ga granitoids in the southern Grenville Province. *Geological Society of America Memoir*, **197,** 163–182.
Raimondo, T., Clark, C., Hand, M., Cliff, J. & Harris, C., 2012. High-resolution geochemical record of fluid–rock interaction in a mid-crustal shear zone: A comparative study of major element and oxygen isotope transport in garnet. *Journal of Metamorphic Geology*, **30,** 255–280.
Schmitt, A.K. & Zack, T., 2012. High-sensitivity U-Pb rutile dating by secondary ion mass spectrometry (SIMS) with an O^{2+} primary beam. *Chemical Geology*, **332–333,** 65–73.
Selleck, B.W., McLelland, J. & Bickford, M.E., 2005. Granite emplacement during tectonic exhumation: The Adirondack example. *Geology*, **33,** 781–784.
Sibson, R.H., Moore, J.M.M. & Rankin, A.H., 1975. Seismic pumping—A hydrothermal fluid transport mechanism. *Journal of the Geological Society*, **131,** 653–659.
Storm, L.C. & Spear, F. S.., 2005. Pressure, temperature and cooling rates of granulite facies migmatitic pelites from the southern Adirondack Highlands, New York. *Journal of Metamorphic Geology*, **23,** 107–130.
Streepey, M., van der Pluijm, B., Essene, E., Hall, C. & Magloughlin, J., 2000. Late Proterozoic (ca. 930 Ma) extension in eastern Laurentia. *Geological Society of America Bulletin*, **112,** 1522–1530.
Streepey, M., Johnson, E., Mezger, K. & van der Pluijm, B., 2001. Early History of the Carthage-Colton Shear Zone, Grenville Province, Northwest Adirondacks, New York (USA). *The Journal of Geology*, **109,** 479–492.
Tiepolo, M., Oberti, R. & Vannucci, R., 2002. Trace-element incorporation in titanite: Constraints from experimentally determined solid/liquid partition coefficients. *Chemical Geology*, **191,** 105–119.
Urey, H., 1947. The thermodynamic properties of isotopic substances. *Journal of the Chemical Society*, 562–581.
Valley, J.W., 2001. Stable isotope thermometry at high temperatures. *Reviews in Mineralogy and Geochemistry*, **43,** 365–402.
Watson, E.B. & Baxter, E., 2007. Diffusion in solid-Earth systems. *Earth and Planetary Science Letters*, **253,** 307–327.
Wiener, R.W., 1983. Adirondack Highlands-Northwest Lowlands "boundary": A multiply folded intrusive contact with fold-associated mylonitization. *Geological Society of America Bulletin*, **94,** 1081–1108.
Wones, D., 1989. Significance of the assemblage titanite+ magnetite+ quartz in granitic rocks. *American Mineralogist*, **74,** 744–749.
Wong, M., Williams, M., McLelland, J., Jercinovic, M. & Kowalkoski, J., 2012. Late Ottawan extension in the eastern Adirondack Highlands: Evidence from structural studies and zircon and monazite geochronology. *Geological Society of America Bulletin*, **124,** 857–869.
Xirouchakis, D., Lindsley, D. & Frost, B., 1998. Equilibria among titanite, hedenbergite, fayalite, quartz, ilmenite, and magnetite; experiments and internally consistent thermodynamic data for titanite. *American Mineralogist*, **83,** 712–725.
Xirouchakis, D., Lindsley, D. & Andersen, D., 2001a. Assemblages with titanite (CaTiOSiO4), Ca-Mg-Fe olivine and pyroxenes, Fe-Mg-Ti oxides, and quartz: Part I. Theory. *American Mineralogist*, **86,** 247–253.
Xirouchakis, D., Lindsley, D. & Frost, B., 2001b. Assemblages with titanite ($CaTiOSiO_4$), Ca-Mg-Fe olivine and pyroxenes, Fe-Mg-Ti oxides, and quartz: Part II. Application. *American Mineralogist*, **86,** 254–264.
Zhang, Y., 2010. Diffusion in minerals and melts: Theoretical background. *Reviews in Mineralogy and Geochemistry*, **72,** 5–58.

SUPPORTING INFORMATION

Additional Supporting Information may be found in the online version of this article at the publisher's web site:

Table S1. Electron microprobe composition data for Harrisville titanite grains.

Table S2. SIMS oxygen isotope data for all Harrisville titanite grains.

Table S3. Oxygen isotope data for titanite standards used in SIMS $\delta^{18}O$ measurement and correction.

Table S4. Chemical composition data for titanite standards used in SIMS $\delta^{18}O$ measurement and bias correction.

Table S5: Whole-rock and mineral-separate $\delta^{18}O$ measurements by laser-fluorination gas-source mass spectrometry for the Harrisville samples.

Figure S1. Bias correction curves for the ten SIMS $\delta^{18}O$ analytical session over which the Harrisville titanite data were collected. The equation for the linear least-squares regression and the associated correlation coefficient are shown for each correction curve. Lowermost right hand plot is a compilation of all the curves for comparison.

Appendix S1. Fast Grain Boundary model and code.

Received 14 July 2013; revision accepted 25 October 2013.